INFORMATION TO USERS

This manuscript has been reproduced from the microfilm master. UMI films the text directly from the original or copy submitted. Thus, some thesis and dissertation copies are in typewriter face, while others may be from any type of computer printer.

The quality of this reproduction is dependent upon the quality of the copy submitted. Broken or indistinct print, colored or poor quality illustrations and photographs, print bleedthrough, substandard margins, and improper alignment can adversely affect reproduction.

In the unlikely event that the author did not send UMI a complete manuscript and there are missing pages, these will be noted. Also, if unauthorized copyright material had to be removed, a note will indicate the deletion.

Oversize materials (e.g., maps, drawings, charts) are reproduced by sectioning the original, beginning at the upper left-hand corner and continuing from left to right in equal sections with small overlaps. Each original is also photographed in one exposure and is included in reduced form at the back of the book.

Photographs included in the original manuscript have been reproduced xerographically in this copy. Higher quality 6" x 9" black and white photographic prints are available for any photographs or illustrations appearing in this copy for an additional charge. Contact UMI directly to order.

UMI

A Bell & Howell Information Company
300 North Zeeb Road, Ann Arbor MI 48106-1346 USA
313/761-4700 800/521-0600

Université d'Ottawa · University of Ottawa

Optical properties of α-$ZnAl_2S_4$:Cr single crystals

by

Isabelle Broussell

Thesis submitted to the School of Graduate Studies
and Research in partial fulfillment of the requirements for the degree of
Master of Science in Physics

Department of Physics
University of Ottawa
150 Louis Pasteur
Ottawa, Ontario
1998

ABSTRACT

The optical properties of the chromium doped spinel type semiconductor α-$ZnAl_2S_4$ have been examined over the temperature range 2-540K. From extrinsic absorption and photoluminescence spectra the transitions between the ground state $^4A_{2g}$ and the excited levels ^2E_g (R_1 and R_2), $^2T_{2g}$, $^4T_{2g}$ and $^4T_{1g}$ of the Cr^{3+} ions were observed. A fit of the measured temperature dependence of the PL decay, using a four level model, yielded the lifetimes of the ^2E_g (R_1 and R_2) and $^4T_{2g}$ levels and the energy gaps between the $^2E_g{}^{(1)}$-$^2E_g{}^{(2)}$ and $^2E_g{}^{(1)}$-$^4T_{2g}$ states which were found to be very close to the values obtained from steady-state measurements. A configurational coordinate diagram for Cr^{3+} ions in a α-$ZnAl_2S_4$:Cr spinel host has been constructed. Optical gain measurements at 198 K, 298 K and 380 K displayed two separate spectral regions associated to the Cr^{3+} ions and possibly to Cr^{4+} impurity centers. Gain values of up to 25 cm^{-1} (730 nm) at 198 K were obtained. Finally the intrinsic photoluminescence measurements revealed an intense UV peak around 380 nm from 20 K to 296 K which corresponds to the indirect band gap of the host crystal, α-$ZnAl_2S_4$.

SOMMAIRE

Les propriétés optiques du semiconducteur de type spinel α-$ZnAl_2S_4$ dopé au chrome ont été examinées sur la plage de température de 2 K à 540 K. À partir des spectres extrinsèques d'absorption et de photoluminescence, les transitions entre le niveau fondamental $^4A_{2g}$ et les niveaux excités ^2E_g (R_1 et R_2), $^2T_{2g}$, $^4T_{2g}$ et $^4T_{1g}$ des ions Cr^{3+} ont été observées. Une équation, obtenue d'un modèle à quatre niveaux, a été ajustée à la dépendance en température des temps de chutes de la luminescence. Les paramètres de l'équation ont fournis les valeurs pour la durée de vie des niveaux ^2E_g (R_1 et R_2) et $^4T_{2g}$ ainsi que les différences d'énergies entre les états $^2E_g^{(1)}$-$^2E_g^{(2)}$ et $^2E_g^{(1)}$-$^4T_{2g}$ qui étaient très proches des valeurs obtenues des spectres d'absoption et de photoluminescence. Un diagramme de configuration pour les ions de Cr^{3+} dans les cristaux de α-$ZnAl_2S_4$ a été construit. Des mesures de gain optique à 198 K, 298 K et 380 K ont démontrées deux régions spectrales associées aux ions de Cr^{3+} et possiblement aux centres d'impuretés Cr^{4+}. Des valeurs de gain jusqu'à 25 cm^{-1} (730 nm) à 198 K ont été obtenues. Finalement les mesures de photoluminescence intrinsèque ont révélé un pic UV intense autour de 380 nm de 20K à 296 K qui correspond à la bande indirecte d'énergie du cristal hôte, α-$ZnAl_2S_4$

ACKNOWLEDGMENTS

I wish to thank Dr. E. Fortin for encouraging me to pursue this project and for his help and support throughout my work. I deeply appreciate the collaboration of Dr. Kulyuk who made this thesis possible by supplying us with the crystals. I would also like to thank Dr. Anedda for the use of his laboratory and his help along with R. Corpino in gathering the intrinsic PL measurements presented in this thesis. Finally I wish to acknowledge the assistance in the experiments of E. Benson and B. Doiron.

STATEMENT OF ORIGINALITY

All the results presented in this thesis on the extrinsic properties of $ZnAl_2S_4$:Cr are from measurements completed at the University of Ottawa by the author in collaboration with Dr. E. Fortin and Dr. L. Kulyuk. The results on the intrinsic properties of $ZnAl_2S_4$:Cr were obtained from measurements completed at the Università di Cagliari in Italy by the author in collaboration with Dr. A. Anedda and R. Corpino. Some of the results printed in this thesis were published in the following papers:

I. Broussell, E. Fortin, L. Kulyuk, S. Popov, Photoluminescence of the Cr^{3+} ions in α-$ZnAl_2S_4$:Cr single crystals, Solid State Communications, Vol. 99, No. 12, pp. 921-925, 1996

I. Broussell, E. Fortin, L. Kulyuk, S. Popov, V. Tezlevan, Luminescence of the Cr3+ ions in spinel type (alpha)-ZnAl2S4:Cr single crystals, to be published in Journal of Luminescence for the proceedings of ICL'96.

I. Broussell, E. Fortin, L. Kulyuk, S. Popov, A. Anedda and R. Corpino, Optical properties of α-$ZnAl_2S_4$:Cr single crystals, submitted to J. of Appl. Physics in november 1997.

Part of the results in this thesis were also presented at the following conferences:

I.Broussell, E. Fortin, L. Kulyuk, S. Popov and V. Tezlevan, Luminescence of the Cr^{3+} ions in spinel type α-$ZnAl_2S_4$:Cr single crystals, presented as a poster at the ICL'96 conference in Prague (August 1996) and at the CAP conference in Ottawa (June 1996).

I. Broussell, Optical properties of α-$ZnAl_2S_4$:Cr single crystals, presented as a talk at the 1997 Fall OCIP graduate students seminars at Carleton University.

TABLE OF CONTENTS

LIST OF FIGURES

LIST OF TABLES

I- INTRODUCTION

A great variety of semiconductors from silicon and germanium to the III-V compounds have been studied in the past because of their multiple applications such as solid state lasers and electronic devices. As the need for more precise applications grows rapidly it is necessary to find materials with adjustable properties and better performance. This is done either by growing new semiconductor crystals or by doping already existing materials with different impurities. A widely studied family in the past few years includes the ternary compounds $A^{II}B_2^{III}X_4^{VI}$ where usually A= Zn, Cd, Hg or Mg, B= Ga or In and X=S, Se or Te. However recently $ZnAl_2S_4$, a novel defective ternary compound belonging also to this family, was successfully grown. We can therefore add aluminum now to the group of elements B from above.

Since $ZnAl_2S_4$ is a defective compound it crystallizes in several crystal structures depending on the conditions of material preparation such as the temperature of synthesis and the Al/Zn ratio. In the low temperature growth region (800-900 °C) $ZnAl_2S_4$ exists in two structures, a defect spinel phase α and wurtzite phase W while at higher growth temperatures (1050-1100 °C) an orthorhombic phase β and a rhombohedral phase γ coexist with the W-phase. The crystal structure of an α-$ZnAl_2S_4$ spinel crystal is illustrated in Figure 1. α- $ZnAl_2S_4$ spinel crystals have been studied recently in a few papers [1, 2] because of their possible application for blue light-emitting devices since they have a band gap in the ultraviolet spectral region. Subsequently a group in Moldova grew single crystals of chromium doped α-$ZnAl_2S_4$ [3]. The optical properties of the resulting new α-$ZnAl_2S_4$:Cr crystals will be the main topic of this research.

The luminescence of the $3d^3$ ion Cr^{3+} in a host crystal as been the subject of many studies because of its application in solid state lasers. It is the optical center in several solid state lasers which operate at room temperature such as the ruby laser (Al_2O_3:Cr) and the alexandrite laser ($BeAl_2O_3$:Cr) [4]. The Cr^{3+} ions interact strongly with the crystal field so the energy gaps between the impurity electronic levels vary from one host crystal

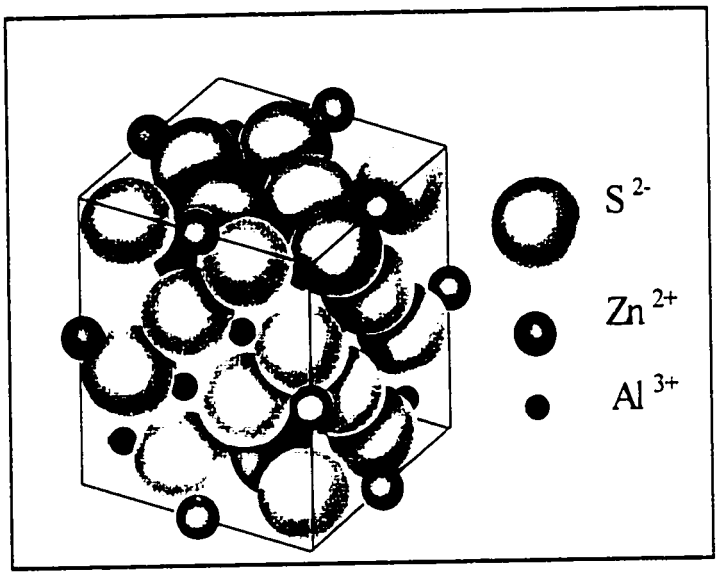

Figure 1 Structure of spinel type crystal taken from ref. [5]

to another. It is therefore of interest to investigate the radiative properties of the Cr^{3+} ions in the novel α-$ZnAl_2S_4$ spinel type crystals. The goal of this work is to realize an analysis of the optical properties of the Cr^{3+} ions in order to determine the suitability of this material for laser application. In addition, since the undoped crystals have not been studied extensively, the intrinsic PL of the host crystal was also investigated.

Drawing an analogy with another chromium doped spinel type semiconductor - $CdIn_2S_4$:Cr, investigated earlier [6, 7], one can expect that the chromium impurity in α-$ZnAl_2S_4$ has to replace the Al^{3+} cations in the octahedrally coordinated sites. On the other hand, the indirect band gap of α-$ZnAl_2S_4$ (E_g(300 K)≅ 3,42 eV [3]) is 1.2 eV larger than for $CdIn_2S_4$ and the lattice constant is smaller (a= 10.01 Å [8]; for $CdIn_2S_4$ a= 10.797 Å [9]) suggesting that the crystal-field for the Cr^{3+} ions in the octahedral sulfur environment of α-$ZnAl_2S_4$ tiospinel should be stronger [10]. Therefore we should observe a substantial shift in the position of the energy levels with respect to those observed in $CdIn_2S_4$:Cr.

The major part of this thesis is devoted to the exploration of the extrinsic properties of α-$ZnAl_2S_4$:Cr. To investigate the chrome impurity levels, extrinsic

absorption measurements were realized at room temperature and at 2- 10 K. Next extrinsic photoluminescence (PL) measurements were completed by exciting the sample under the indirect band gap of α-$ZnAl_2S_4$. The extrinsic PL dependence on temperature and on excitation intensity was also investigated. From the PL spectra we observed the luminescence due to the chrome impurities from 2 K to 530 K and at high temperatures (T> 300 K) we also observed an IR band due possibly to a Cr^{4+} center in the host crystal. In addition the project involved the analysis of PL time resolved measurements to characterize the radiative recombination processes by which the electrons decay. The time decay dependence on temperature was fitted to an equation obtained from a four level model from which we obtained the lifetime and energy gaps of the relevant Cr^{3+} ion states. The time decay dependence on excitation intensity was also verified and showed a sudden drop at a critical intensity.

Finally gain measurements were taken at 198 K, 298 K and 378 K to determine the potential of these materials for laser action. It was hoped to find the presence of optical gain at temperatures above 300 K, but the optical gain due to the Cr^{3+} centers was small at high temperatures. However from preliminary results we observed some gain at 378 K which we attributed to the Cr^{4+} ions in the host crystal. The last section of the present work investigates the intrinsic properties of the samples in the temperature range 10-300 K using PL measurements. By exciting in the direct band gap it was possible to observe emission from the indirect band gap.

The thesis is divided into five chapters the first being the introduction. In the second chapter we start by reviewing the theory required for the analysis of the experimental results. A short introduction to ligand field theory is presented followed by a description of a single configuration coordinate diagram for Cr^{3+} ions in a octahedral crystal field. This model for the energy levels due to the chromium impurities will provide a basis for the explanation of the results obtained from the extrinsic measurements. A summary on the processes involved in optical absorption and PL will ensue. When optical absorption and PL are used as optical probing techniques they can give important

information on the energy levels of the impurity. Next a kinetic model is derived which will be used to describe the temperature dependence of the PL decay times. That chapter ends by treating optical gain.

Chapter III is concerned with the experimental techniques used. The materials studied will be presented and the experimental setups for optical absorption, extrinsic PL, time-resolved, gain and intrinsic PL measurements will be described along with the equipment used. Finally in the principal section of the thesis, Chapter IV, the results obtained from measurements realized on $ZnAl_2S_4$:Cr are presented and discussed; the chapter is divided into six sections: Optical absorption spectra; Extrinsic PL spectra; PL vs Intensity; Time-resolved measurements, Gain measurements and PL of host crystal. We shall then end the thesis with some concluding remarks in Chapter V.

II- THEORY

2.1 Ligand Field Theory

The temperature dependence and the kinetics of the photoluminescence (PL) rely on the relaxation process of the crystal from its excited states to the ground state. In $ZnAl_2S_4$:Cr the electronic states involved in the luminescence are due for the most part to the Cr impurity and they are approximated in terms of the energy levels of the Cr^{3+} ions perturbed by the crystal field. These energy levels derive from the strong interaction of the 3d electrons with the electrostatic field of the host crystal. With the ligand field theory [11, 12] the energy terms can be calculated as a function of the crystal field strength.

The subject of ligand field theory consists of the correlation of the physical properties of an ion or atom with the nature and positions of its nearest neighbors. The nearest neighbors which surround the central ion are referred to as the ligand atoms. The problem resolves itself into first summing the potentials from the individual ligand ions to give the total potential at any point near the central ion, and then finding the effect of such a potential on the electrons of that ion.

Ligand field theory has proven very useful for the discussion of the properties of transition metal compounds. Its applications include thermodynamics, spectral and magnetic properties. In this study we shall be concerned mainly with the interpretation of optical spectra. From the theory we can obtain a treatment of vibrational motions and the electronic transitions within orbitals located on the central ion which in our case is a Cr^{3+} ion. The Cr^{3+} ions in α-$ZnAl_2S_4$:Cr are located in an octahedral field in which there are six ligands located near the vertices of a regular octahedron. The ligand ions consists of zinc ions as seen in Figure 1, since the chromium atoms are thought to replace the Al^{3+} ions in the crystal lattice.

The energy terms have been calculated for all combinations of electrons in octahedral symmetry by Y. Tanabe and S. Sugano [10]. Essentially they treat the active atom, Cr^{3+} in our case, and its six nearest neighbors as a molecule and then determine the energy differences between any of the levels by calculating all the various energy terms in an energy matrix. To apply the theory to the analysis of experiments, the energies of the states were plotted as a function of parameters, involved in the energy matrix, in a Tanabe-Sugano diagram which is shown on Figure 2. The diagram is for three electrons in a 3d subshell which is the case for triply ionized chrome. The energy of the levels and the crystal field strength are expressed in terms of the Racah parameter B and the crystalline field parameter Dq. B is a value introduced by Racah as a measure of the electron interaction and can be expressed in terms of Slater integrals. The field strength parameter Dq is a function of the separations , charges and dipole moments of the ions, which have uncertain values. It is therefore not possible to carry out absolute calculations of Dq values for specific complexes; rather Dq is obtained from absorption spectra.

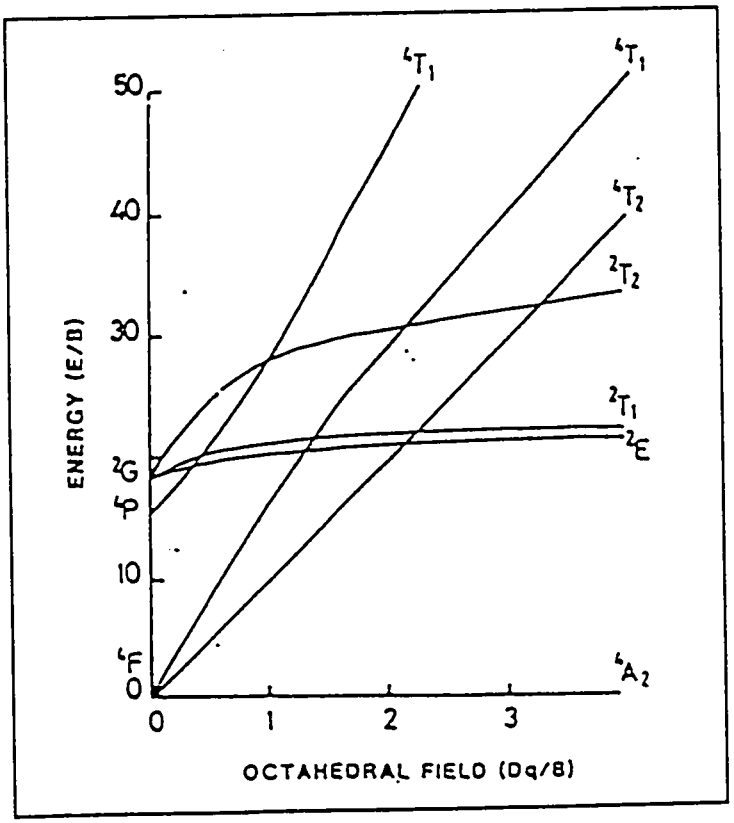

Figure 2 Tanabe-Sugano diagram for the Cr^{3+} ions in octahedral crystal fields. The energies E and Dq have been scaled by the inter-electron energy B. The figure is taken from ref. [10].

Absorption or emission occurs when an electron makes a transition between levels. The energy of the absorbed or emitted photon depends on the energy difference between the initial and final state of the electron. In purely electric dipole transitions all the energy involved in the transition is either absorbed from a photon or emitted into a photon. However phonons, from crystal lattice vibrations, can also participate in the transitions. To determine which kind of transition between two levels will be strongest we can refer to selection rules. If a transition is allowed it will obviously have a stronger absorption or emission spectrum.

For transition metal ions two selection rules are important; the spin and Laporte selection rules. The first selection rule indicates that a transition can only occur between levels in which the number of unpaired electrons in the initial and final states is the same. Also when a single electron undergoes a transition the spin of the initial and final states must be the same. According to the Laporte selection rule [11], a transition is forbidden if it involves only a redistribution of electrons having similar orbitals within a single quantum shell. This is relevant to transition metal ions since the transitions are often between 3d levels and within the same quantum shell.

Usually the strongest interaction which allows a transition is the electric dipole interaction but not in transition metal ions since for the 3d electrons all levels have the same parity so all transitions between those levels are forbidden. In transition metal ions the strongest interaction is the electric dipole transition coupled with a vibronic transition. A vibronic transition involves the simultaneous absorption or emission of both photons and phonons. The strengths of the electric quadrupole interaction and the magnetic dipole interaction were also estimated but were found to be more than 2 orders of magnitude smaller by Tanabe and Sugano.

In the diagram in Figure 2 each energy level is labeled by a term of the form $^{2s+1}X_g$. The S represents the spin quantum number and the g index is used to indicate that in octahedral complexes there is the presence of a center of symmetry. The term X is related

to the symmetry of the site of the active ion and it is represented by letters which come from group theory and are associated with character tables describing the group. For triply ionized chrome the ground state is always represented by $^4A_2$, however the first excited state depends on the crystal field strength. As seen from Figure 2, as the crystal field changes the splitting between levels can change substantially which is why the properties of chromium atoms can vary greatly between crystal hosts.

Table I Nomenclature of absorption transitions

Absorption	Transitions
R lines	$^4A_{2g} \rightarrow {}^2E_g$
R' lines	$^4A_{2g} \rightarrow {}^2T_{1g}$
U band	$^4A_{2g} \rightarrow {}^4T_{2g}$
B lines	$^4A_{2g} \rightarrow {}^2T_{2g}$
Y band	$^4A_{2g} \rightarrow {}^4T_{1g}$

Finally from the selection rules and the properties of the energy levels each absorption transition was given a nomenclature as shown in Table 1. From this it is seen that the transition from the ground state to the ^2E_g state gives rise to the R-lines. In some host crystals further splitting of the transition $^4A_{2g} \rightarrow {}^2E_g$ into R_1 and R_2 lines can occur because of low field symmetries. This transition is spin forbidden and gives rise to narrow spectral features whereas the spin allowed transitions give rise to the Y and U band which have wide spectral features. This will be observed in our results latter. The parameter 10 Dq is defined as the energy associated with the U-band, that is the energy from the transition $^4A_{2g} \rightarrow {}^4T_{2g}$ obtained from the absorption spectra. The Racah parameter B can also be obtained from the absorption spectra with the following relation [13]

$$B = \tfrac{1}{3} \frac{(20Dq - h\nu)(h\nu - 10Dq)}{90Dq - 5h\nu} \qquad (1)$$

where hυ represents the energy for the transition $^4A_{2g} \rightarrow {}^4T_{1g}$. These parameters for the case of triply ionized chrome in $ZnAl_2S_4$ will be determined from our measurements in section 4.1.

2.2 Configuration Coordinate Diagram

To get a better picture of the processes involved in the various optical transitions due to the Cr^{3+} ions, the energy terms determined in the previous section and summarized in the Tanabe-Sugano diagram can be plotted as a function of a configuration coordinate. In a single configurational coordinate model, the interaction of the active atom and its nearest neighbors is described by a single configurational parameter. This configurational parameter describes one aspect of the geometrical configuration of the active atom with its nearest neighbors. For example in the case of the Cr^{3+} ions in octahedral symmetry the configurational parameter can be the distance between the chromium atom and its nearest neighbors. Therefore as the single configurational coordinate changes the average distance of the chrome atom and its six nearest neighbors expands or contracts.

From Figure 2 we can construct the single configuration coordinate diagram for the Cr^{3+} ions in the α-$ZnAl_2S_4$ spinel host crystal as shown on Figure 3. Since the chromium atoms in α-$ZnAl_2S_4$ are expected to be in a strong field the lowest excited level (as seen on Figure 2) is ^2E_g. The Δ_1 and Δ_2 gaps represent respectively the energy values between the minima of the $^2E_g^{(2)}$ and $^4T_{2g}$ parabolas and the $^2E_g^{(1)}$ parabola. The ^2E_g state is split into $^2E_g^{(1)}$ and $^2E_g^{(2)}$ and the $^2T_{1g}$ state is not shown since it does not usually appear in emission spectra. $h\upsilon_1$, $h\upsilon_2$ and $h\upsilon_3$ correspond to radiative transitions from $^2E_g^{(1)}$, $^2E_g^{(2)}$ and $^4T_{2g}$ to the $^4A_{2g}$ ground state respectively. These values will be determined in section 4.1-4.2 from absorption and photoluminescence measurements. The configuration coordinate diagram will be useful for interpreting qualitatively the temperature and intensity dependence of the extrinsic emission results.

The equilibrium positions are located near the lowest points in the parabolas since energy is required to either expand or contract the configurational coordinate. For example if the distance between the Cr^{3+} ions and the ligand atoms decreases, their mutual repulsion will tend to push them apart. The strength of the interaction determines the curvature of the parabolas. If the energy depends weakly on the configurational coordinate then the parabola will be weakly curved and conversely if the dependence is strong the curvature will be strong. The curvature for different energy levels can vary but we can assume the force constants of all the potential wells to be equal [14], as we did for the diagram in Figure 3. Parabolas for different levels can also be offset, meaning the equilibrium positions can occur at different values of the configurational coordinate. Different energy levels have different electric charge configurations so the equilibrium position of the nearest neighbors can vary.

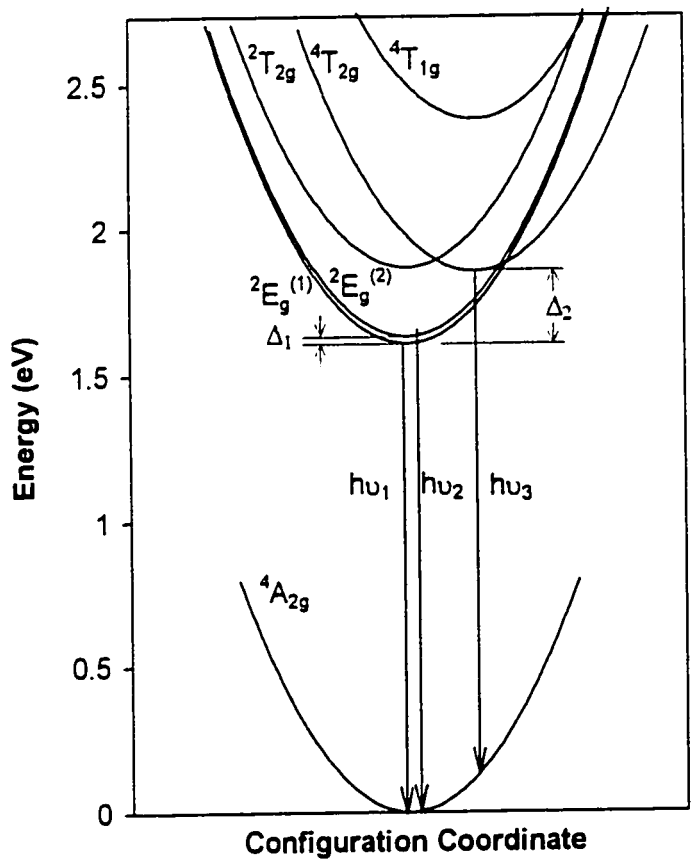

Figure 3 Single coordinate configuration diagram of the Cr^{3+} ions in α-$ZnAl_2S_4$, showing the relevant energy levels and optical transitions.

2.3 Absorption & Photoluminescence

From photoluminescence (PL) and absorption measurements it is possible to determine the energy between different states in a crystal, such as those in Cr^{3+} ions as seen in the previous two sections. These two experimental techniques have been widely used in the study of semiconductors, absorption measurements being the most popular tool in the past. However recently PL has become more widely used because of the increased accessibility of tunable sources for excitation. Also this technique is simpler than absorption and can be applied on samples of any size and only one good optical surface is needed. Nevertheless since certain spectral features will be strong in one technique and weak in the other and vice versa, to obtain all the spectral features, PL and absorption are used as complementary techniques.

Absorption occurs when the incident light excites an electron to a higher energy state in a physical system and luminescence occurs when the decaying process of the electron is radiative. In particular PL is the process were optical radiation is emitted when the excitation comes from optical absorption. Therefore PL is the inverse process of absorption. There can also be luminescence from other excitation mechanisms such as electroluminescence, cathodoluminescence, thermoluminescence and triboluminescence. When the exciting light is strongly absorbed then most of the excitation of the sample will occur near the front surface. Therefore if the absorption coefficient is large the luminescence will be mostly constrained to the front surface. This is why the vast majority of PL experiments are arranged to examine the light emitted from the irradiated side of the sample which is called front surface luminescence.

For example if we consider the single configuration coordinate diagram for Cr^{3+} (Figure 3), a photon whose energy is equal or greater than the energy between the ground level and the first excited state can excite the electrons from the ground state $^4A_{2g}$ to higher states. The transitions are vertical and when the final state is offset from the bottom of the parabola the electron relaxes down to the equilibrium position. If the return

process when the electron relaxes back to the ground state is radiative, then it emits a photon whose energy gives the difference between the excited state (not necessarily at the bottom of the parabola) and the ground state energy such as $h\upsilon_1$, $h\upsilon_2$ and $h\upsilon_3$. So the emission spectrum will show a peak related to the energy of each excited states whose intensity depends on the strength of the transition. There are also radiationless transitions that compete with the radiative transitions and therefore also affect the emission spectrum. The importance of the radiationless processes increases with temperature since more energy is available to the electrons through vibrations in the crystal (phonons).

2.4 Kinetic model

In order to describe the temperature dependence of the PL decay a simplified four levels kinetic model [15] was used (Figure 4). The three excited levels $^2E_g^{(1)}$, $^2E_g^{(2)}$ and $^4T_{2g}$ were assumed to be in quasithermodynamic equilibrium and the radiationless transitions to the $^4A_{2g}$ ground state were neglected. The γ's and the W's represent the transition probabilities between the energy states by radiative and non-radiative processes respectively. If N_j represents the population of state j then the equations governing the system are

$$\begin{cases} \dfrac{dN_1}{dt} = -(\gamma_1 + W_{12})N_1 + W_{21}N_2 \\ \dfrac{dN_2}{dt} = -(\gamma_2 + W_{21} + W_{23})N_2 + W_{12}N_1 + W_{32}N_3 \\ \dfrac{dN_3}{dt} = -(\gamma_3 + W_{32})N_3 + W_{23}N_2 \end{cases} \qquad (3)$$

where W_{13} and W_{31} were neglected since the nonradiative transitions $^2E_g^{(1)} \rightarrow {}^4T_{2g}$ and $^4T_{2g} \rightarrow {}^2E_g^{(1)}$ should be negligible compared to the transitions $^2E_g^{(1)} \rightarrow {}^2E_g^{(2)}$ and $^4T_{2g} \rightarrow {}^2E_g^{(2)}$ respectively. The W_{ij} and W_{ji} terms are related by the following relation:

$$\frac{W_{ij}}{W_{ji}} = \frac{g_i}{g_j} e^{-\Delta_{ij}/kT} \tag{4}$$

where Δ_{ij} is the energy gap between state i and j and the g's represent the degeneracy of each state. The levels $^2E_g^{(1)}$, $^2E_g^{(2)}$ and $^4T_{2g}$ have a degeneracy of 2, 2 and 12 respectively.

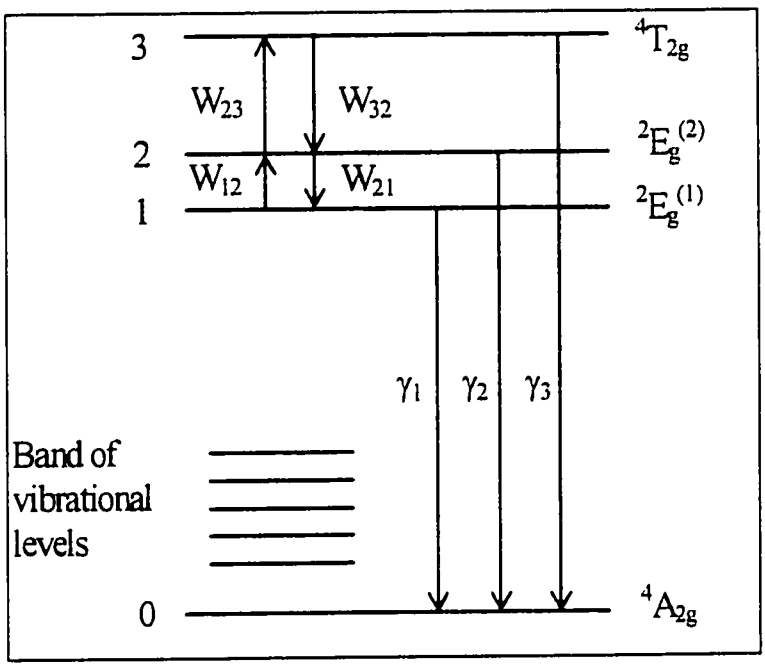

Figure 4 The four-level model for Cr^{3+} luminescence in a high crystal field.

We then assume a solution of the form $N_j=\alpha_j e^{-t/\tau}$,where τ is the decay time constant and α is a constant, which we insert in the system of equations (3). We also substituted the γ's by the inverse of the lifetimes of each state since $\gamma_i = \tau_i^{-1}$ using the following notation: $\tau_{E1} = \gamma_1^{-1}$, $\tau_{E2} = \gamma_2^{-1}$ and $\tau_{T2} = \gamma_3^{-1}$ where τ_{E1}, τ_{E2} and τ_{T2} are the lifetimes of the $^2E_g^{(1)}$, $^2E_g^{(2)}$ and $^4T_{2g}$ states respectively. By solving the resulting equations using the same approach as in ref. [16, 17] and assuming that the nonradiative transition rates from excited states are small in comparison with those of radiative transitions, then we obtain the following expression for the luminescence decay time of the Cr^{3+} ions as a function of temperature

$$\tau(T) = \tau_{E1} \frac{1 + e^{-\Delta_1/kT} + 6e^{-\Delta_2/kT}}{1 + (\tau_{E1}/\tau_{E2})e^{-\Delta_1/kT} + (6\tau_{E1}/\tau_{T2})e^{-\Delta_2/kT}} \qquad (5)$$

where k is the Boltzmann's constant, Δ_1 and Δ_2 ($\Delta_1 = \Delta_{21}$, $\Delta_2 = \Delta_{32}$) are as defined previously (Figure 3). The degeneracy ratio of $^4T_{2g}$ to that of ^2E_g [1] (6) has also been taken into account.

2.5 Three-level and four-level laser

Since optical gain measurements were realized in the course of this work it is necessary to have a good understanding of the conditions under which lasing can occur. In the simplest case we can have a three-level laser system like the ruby laser or a four-level like laser system like the alexandrite laser. In each of these two lasers the active laser medium is the Cr^{3+} ions which suggest lasing could also occur in α-$ZnAl_2S_4$:Cr.

The three level operating scheme is illustrated in Figure 5 where the levels involved are the ground level which acts as the lower laser level, the pump level and the upper laser level. The pump photon excites the electron from the ground state into the pump level. It then relaxes rapidly to the upper laser level and a laser photon is emitted as the electron relaxes back to the ground state. For stimulated emission and eventually lasing to occur the population density of the upper laser level has to be greater than the population density of the lower laser level. When this situation occurs a population inversion is said to exist. To achieve a population inversion, more than half of the Cr atoms must be pumped to the upper level. For this to occur the rate of pumping must be greater than the rate of spontaneous transition from the upper laser level to the ground state. In other words the pumping rate must be high or the lifetime of the upper laser level must be long. Laser action can occur when population inversion is achieved and can be sustained as long as the population inversion is maintained.

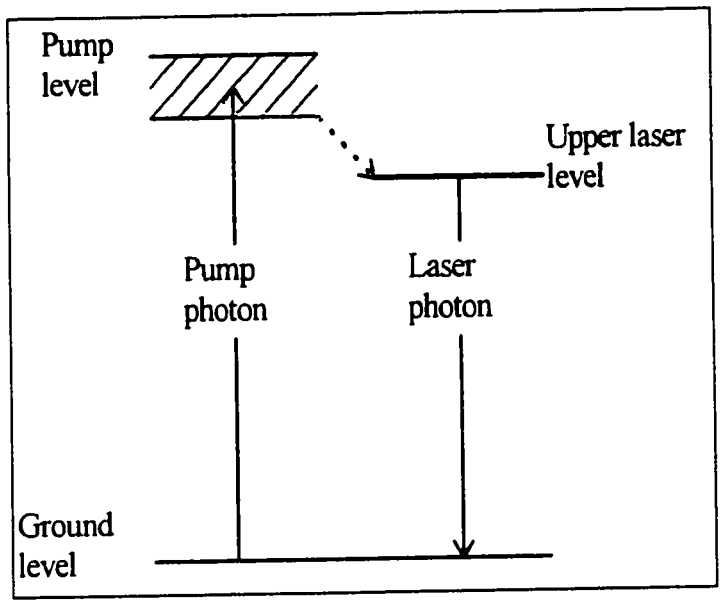

Figure 5 Three-level laser energy-level diagram.

In the ruby laser the upper laser level is ^2E_g and the lower laser level is the ground state $^4A_{2g}$. The ruby laser operates with a narrow linewidth at 694 nm, at the border of the visible spectrum. However the three-level laser is relatively inefficient because it needs a great deal of pump energy to store enough energy in the upper laser level to achieve population inversion. Furthermore only the portion of energy stored in the upper laser level which is above threshold participates in the laser output.

Let us now consider a four-level laser as depicted in Figure 6. A four-level laser has a ground level, a pump level and an upper laser level, similar to the three-level laser, in addition to a fourth level which acts as the lower laser level. As with the three-level laser the lasing occurs between the upper laser level and the lower laser level but with four-level operation this last level is above the ground state. Therefore the lower laser level has virtually no population density to begin with. Furthermore when the electrons decay to the lower laser level they quickly relax back to the ground state therefore emptying the lower laser level. Since the lower laser level is virtually empty the threshold is much easier to achieve. Consequently for the four-level laser the population density of the ground state does not need to be overcome as with the three-level laser.

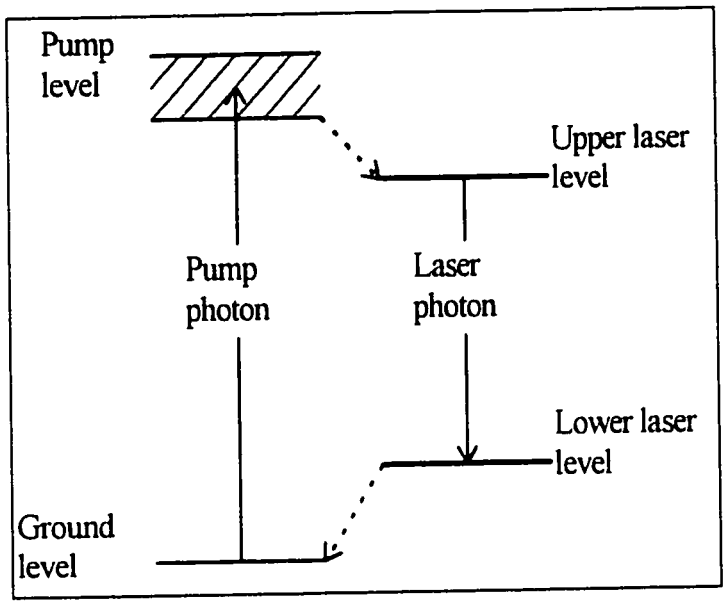

Figure 6 Four-level laser energy-level diagram.

The alexandrite laser is not a true four-level laser but it operates on a vibronic transition which resembles the four-level like operation. In that laser the ground state is still $^4A_{2g}$ but the upper laser level is $^4T_{2g}$ and the lower laser level is a virtual vibronic state which acts as the lower laser level. As was seen previously from the configuration coordinate energy-level diagram presented in Figure 3, the $^4T_{2g}$ state is offset from the equilibrium position of the ground state which implies the transition $^4T_{2g} \rightarrow {}^4A_{2g}$ must be completed by phonon emission. From optical gain measurement it will be possible to determine which of these two schemes, three-level or four-level laser operation, is present in our α-$ZnAl_2S_4$:Cr crystals by finding through which transition optical gain occurs. The transition from the ^2E_g state implies the three-level scheme with narrow linewidth emission whereas the transition from the $^4T_{2g}$ state implies the four-level scheme with a large vibronic emmision.

2.6 Optical Gain

This section will show how to determine the gain coefficient with a relatively simple experiment and that this gain coefficient is directly related to the degree of population inversion. If a beam of light with frequency υ is incident on a semi-conducting medium where there is an inversion of population between two levels with an energy difference of hυ, then the incident beam will trigger the stimulated emission and amplification will occur. This situation is presented in Figure 7 where z is the direction of propagation of the light beam and dz is the differential element of the medium considered.

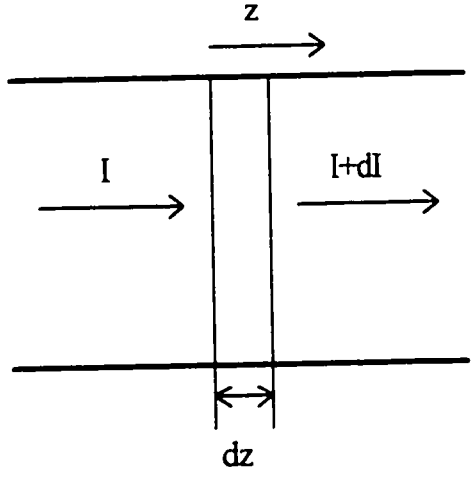

Figure 7 Stimulated emission in the gain material

If the incident light beam has an intensity I, then it will have an intensity I+dI when it is re-emitted by the differential element dz such that dI α I dz. Therefore by multiplying Idz by a constant of proportionality g we obtain

$$dI = gIdz \tag{6}$$

where g is the optical gain coefficient of the medium considered. When g is negative there is absorption in the medium whereas when g is positive there is amplification. By integrating equation (6) we obtain an expression which gives the intensity of the beam as a function of the thickness z of the amplification medium:

$$\int_{I_o}^{I} \frac{dI}{I} = \int_{o}^{z} g dZ$$

$$I = I_o e^{(gz)} \qquad (7)$$

where I_o is the intensity of the incident beam.

We shall now consider the principles involved in optical gain measurements. This is summarized in Figure 8 where a narrow beam of length z is incident on the medium and the PL is observed along the z axis, perpendicular to the exciting beam. The length of the excited region is varied from z to z+dz. If I_s is the rate of spontaneous emission by unit volume then the region of volume Adz will contribute a spontaneous emission intensity I_sAdz to the total PL in the direction of the excited region along the z axis. Therefore the I_o in equation (7) corresponds to I_sAdz and the change in the stimulated emission when the

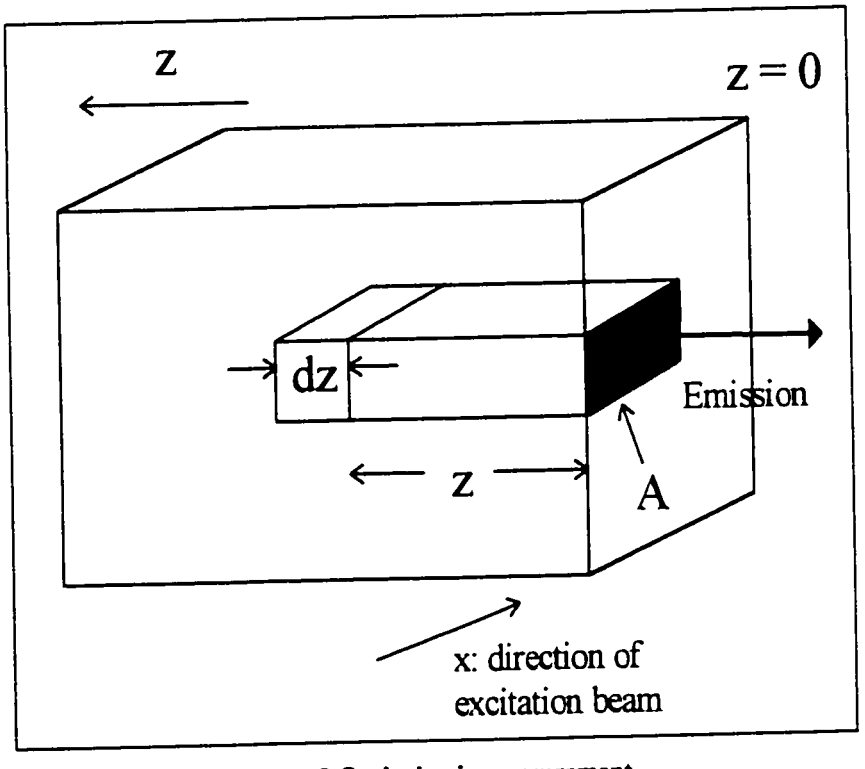

Figure 8 Optical gain measurement.

photons propagate in the excited region is given by

$$dI = I_s A e^{(gz)} dz \tag{8}$$

Now if the length z of the excited region is varied from 0 to l, by integrating equation (8) we can obtain the total stimulated emission intensity I(l):

$$\int_0^{I(l)} dI = \int_0^{l} I_s A e^{(gz)} dz$$

$$I(l) = \frac{I_s A}{g}(e^{(gl)} - 1) \tag{9}$$

where $I_s A$ is the rate of spontaneous emission times the surface aria of the emitting region. Therefore by measuring the stimulated emission intensity as a function of the excitation length it is possible to obtain the optical gain coefficient by fitting the results to equation (9). This technique was first used by Shaklee [18] and the experimental setup for optical gain measurements will be further described in section 3.3.

III- EXPERIMENTAL TECHNIQUES

This chapter will treat the experimental part of this research. First a short discussion on the samples studied is presented. Section 3.2 contains the summary for three experiments: optical absorption, PL and time-resolved measurements. It also includes a description of the characteristics of the experimental optical system for which the PL spectra must be corrected. Then in section 3.3 the optical gain setup will be presented. The last section of this chapter deals with the experimental setup and the instruments used for the intrinsic PL experiment.

3.1 α-$ZnAl_2S_4$:Cr

The single crystals of chromium doped α-$ZnAl_2S_4$ were grown in Moldova [19] by a closed tube vapor transport method with iodine as a transport agent. The samples obtained were optically uniform octahedra with dimensions up to 30 mm^3 and (111) oriented mirror like faces. The samples which have a transparent light green appearance have an estimated Cr-impurity concentration in the region of 0.1-0.3 at %. The crystalline lattice of the crystal host studied possesses a structure of a normal spinel as confirmed by X-ray analysis [20].

Two of the samples had to be polished for absorption and gain measurements. The first technique requires two parallel faces of good optical quality while the second technique requires two perpendicular faces of good optical quality. The samples were polished simply by rotating the crystal with a finger on a glass plate covered with a wet 1 μm polishing powder. The crystals were too small to mount on a holder and they scratched easily.

3.2 Experimental setup

The general experimental setup is shown in Figure 9. This figure includes the geometry for three different experiments; optical absorption, steady-state PL and PL time-resolved measurements. The common features of these experiments will first be described followed by the specific details in the next four subsections. The gain apparatus will be discussed in the next section.

In all cases the light output from the sample, located at the center of Figure 9, is picked up by a first lens at a distance from the sample equal to its focal length. This lens usually had a focal length of 12.5 cm as labeled in the figure however it could also be changed if needed to vary the focal length between 10 cm to 20 cm depending on how close we could fit the lens to the sample holder. The closer it is to the sample the more light can be collected but the sample was sometimes placed in a temperature controlled container which limited the distance at which the lens could be placed. The second lens, with a focal length of 15 cm, focuses the light into a 1m grating monochromator. Finally the light output of the spectrometer was detected with a Hamamatsu R-636 photomultiplier with a GaAs photocathode operating with a high voltage source of 1250 V. The resolution at the output of the spectrometer could be varied from 2- 16 Å depending on the width of the entrance and exit slit which could be set up to 2 mm. The optical response of the spectrometer and the photomultiplier is reviewed in section 3.2.3.

For room temperature measurements the sample was mounted on a rotation stage. To obtain lower temperatures (2-300K) the sample was placed in a Janis variable temperature liquid helium optical cryostat with independent sample chamber. The cryostat had four optical windows and the temperature readings were supplied by two sensors, one below and one above the sample. The sensors were silicon diodes which have a temperature calibrated resistance. The upper sensor was closer to the sample but the accuracy was limited by a temperature gradient in the gas and liquid phases. To vary the temperature a heater placed below the sample was used. The pumping speed on the He

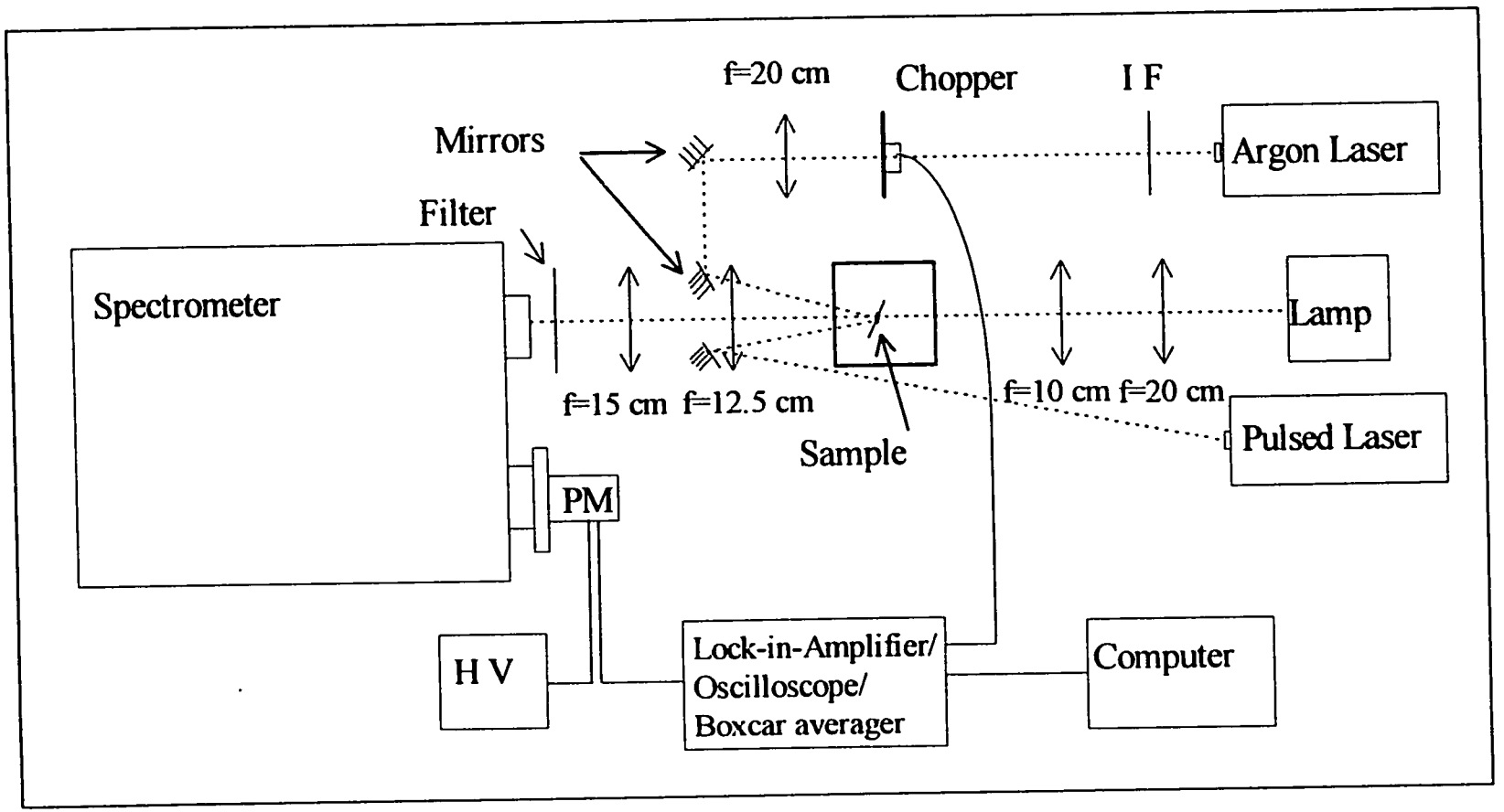

Figure 9. Experimental setup used for steady-state, time-resolved photoluminescence and optical absorption measurements.

gas and the liquid He flow to the sample chamber can also be varied to maintain a certain temperature. At 2 K the sample was in superfluid liquid helium and for higher temperatures it was in helium gas. For temperatures between 200- 300 K liquid nitrogen was used instead of liquid He since it was more readily available.

To achieve temperatures above 300 K and up to 530 K, a standard Black and Decker household mini-oven was employed, complete with large optical access and a temperature regulation better than ± 5K at 530 K. The oven however was bulky and took up a lot of room which left a very narrow field for the optical adjustments. Furthermore it was difficult to adjust the position of the sample since the oven was hard to handle. At high temperatures is was particularly difficult to displace the oven since it became extremely hot and furthermore upon heating, the sample or the oven's position would change slightly making new adjustments necessary. To maintain the sample in place on the sample holder we used silicone adhesive sealant which worked well at all temperatures studied.

3.2.1 Optical absorption

For absorption measurements the setup in the center of Figure 9 is used, from the lamp to the spectrometer. The sample was placed in the cryostat so that absorption measurements at 2, 10 and 300 K could be realized. A sample with two parallel faces was used. It was placed on a support which had a small hole in it ($d < 1$ mm) to let the light from the lamp pass through the sample. Two lenses were used to collect the light beam from a quartzline lamp and then focus it onto the hole where the sample was placed. A chopper was placed between the lamp and the sample to allow detection of the transmitted light with a Stanford Lock-in-Amplifier. The transmitted intensity was then collected as a function of wavelength by the photomultiplier and the data was registered on the computer.

To find the actual absorption spectra we also needed to take a reference spectrum by removing the sample since the light distribution of the lamp and the light response of the spectrometer and the detector are not spectrally uniform. The absorption coefficient, α, is given by the relation

$$I = I_o e^{-\alpha d}$$

$$\alpha = \frac{1}{d} \ln\left(\frac{I_o}{I}\right) \qquad (10)$$

where d is the thickness of the sample and I and I_o are the transmitted and incident intensities respectively. The absorption spectrum was then obtained by taking the natural logarithm of the reference spectrum divided by the transmitted spectrum of the crystal. However this will not give the absolute absorption coefficient since we did not consider the thickness of the sample but we are only interested in the spectral features of the absorption and not in its absolute value.

3.2.2 Photoluminescence

To obtain the PL emission spectra of $ZnAl_2S_4$:Cr, a fixed wavelength is used as the exciting source while the radiation coming off the sample at different wavelengths is recorded. These measurements allow us to determine the energy of the transitions involved in the recombination processes. The setup used for the PL measurements is presented in the upper part of Figure 9. The excitation source for the steady-state PL was the 514.5 nm line of an argon laser which excited the Cr^{3+} ions in the Y absorption band as will be seen from the absorption results in section 4.1. An interference filter was placed in front of the beam to let pass only the main laser line. This was done to eliminate the weaker Argon plasma lines which showed up in the PL spectra when the luminescence was relatively weak.

The exciting beam then passed through a chopper and a lens that focused it onto the sample. The area of the beam thus obtained on the sample was in the order of 10^{-7} m^2. Mirrors were used to redirect the beam so that it hit the sample near normal to its surface. The front surface luminescence emitted by the sample was then picked up by two lenses and focused into the spectrometer. A high pass optical filter (Hoya color filter O-56) was placed between the sample and the spectrometer to prevent the stray light of the laser from entering the spectrometer. If the scattered laser light entered the spectrometer it could reach the detector and even saturate it. The filter used eliminates all wavelengths below 540 nm and had a transmission of more than 90 % for wavelengths over 580 nm. A green polarizer was also placed in front of the entrance slit of the spectrometer. The reason for the use of a polarizer will be explained in the next section. The luminescence was then detected by the photomultiplier and the data was collected with a lock-in amplifier and transferred to a computer which registered the signal as a function of wavelength.

For measurements of the PL dependence on the exciting intensity, neutral density filters were used to vary the intensity of the argon laser beam. They were placed between the chopper and the lens which focused the beam on the sample. To obtain even higher intensities we used the argon laser in the multiline mode. That is the 514.5 nm line of the argon laser was used in conjunction with the 488 nm line and a few other less intense lines in the same region. With this setup a maximum intensity of about 4.2 MW/m^2 could be achieved. However the samples were damaged when subjected to this intensity at high temperatures ($T > 300$ K).

3.2.3 Characteristics of the experimental optical system

For the extrinsic PL experiments the measured spectra obtained need to be corrected for the characteristics of the experimental optical system. The spectral response of the photomultiplier and the spectrometer can greatly influence the observed PL spectra if we do not normalize them. To characterize the response of each element a quartzline

lamp, a green polarizer ($\lambda > 400$ nm) and a flat response pyroelectric detector were used. First the light from the lamp was focused on the entrance slit of the spectrometer using a concave miror with a focal length of one meter. Then a spectrum was taken with the pyroelectric detector. By dividing the resulting spectrum by the spectral response of the lamp we obtained the spectrometer's spectral response. The lamp's spectral response was obtained from the blackbody equation:

$$M_e = \frac{2\pi hc^2}{\lambda^5}\left[\frac{1}{e^{hc/\lambda kT} - 1}\right] \tag{11}$$

where M_e is the exitance (total radiant flux density), h is Planck's constant, c is the speed of light, k is Boltzmann's constant, λ is the radiated wavelength and T is the blackbody temperature. The blackbody temperature of the quartzline lamp was taken to be 3000 K [21] to obtain the spectral curve of the lamp.

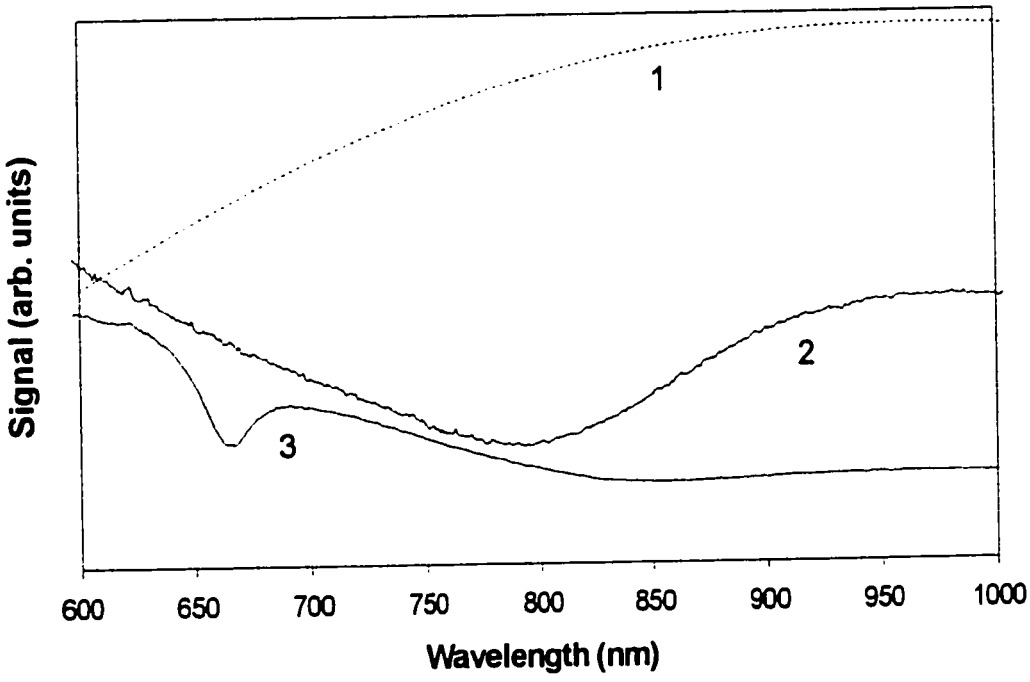

Figure 10 1: Response of the lamp corresponding to the blackbody equation with a temperature of 3000 K. 2: Spectrometer response for vertically polarized light. 3: Spectrometer response for unpolarized light.

The corrected spectrometer response thus obtained is shown in Figure 10 along with the response of the lamp. The lamp response shows part of a blackbody curve with a maximum near 970 nm. The spectrometer response with no polarizer displays two deep indentations around 570 nm (not shown in Figure 10) and 670 nm. These features are undesirable since they create peaks around 650 nm and 700 nm which are difficult to eliminate from our PL spectra. The indentations in the spectrometer response are caused by selective polarization of the incident light induced by the entrance slits and the particular grating used. Fortunatly the spectrometer response for vertically polarized light does not show any sharp indentations, only a large valley is observed around 800 nm. This valley appears because the polarizer starts to lose efficiency in the IR, letting horizontally polarized light pass as well. Therefore by using a polarizer to let only vertically polarized light pass through the spectrometer, the effect of the spectrometer on the detected PL (which was found to be unpolarized) will be kept to a minimum.

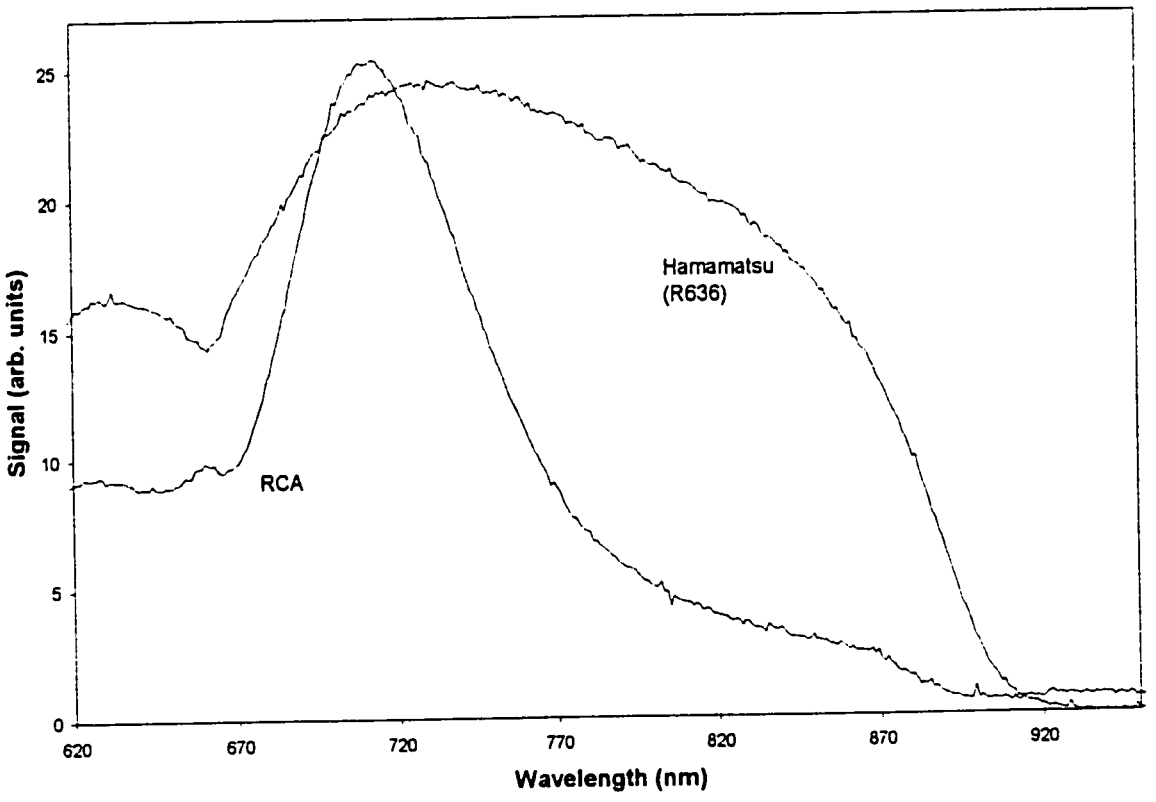

Figure 11 Spectral response of RCA and Hamamatsu (R636) photomultiplier

Next we determine the characteristics of the photomultiplier by using it to detect the spectrum of the lamp through the spectrometer and then correcting it with the convolution of the lamp and spectrometer. This was done for the Hamamatsu (R636) and the RCA photomultipliers to determine which of these had the best spectral characteristics. The spectral responses obtained for the two photomultipliers are shown in Figure 11. The response of the Hamamatsu corresponds to the company's specifications but the RCA shows a very strong and narrow peak suggesting it was damaged. Both photomultipliers stop detecting for wavelengths higher than 900 nm but the RCA's response diminishes more rapidly.

Following these results a green polarizer was placed before the entrance slit of the spectrometer and the Hamamatsu was used to detect the vertically polarized PL. The resulting spectra could then be corrected for the photomultiplier's and the spectrometer's response. Figure 12 displays the convolution of the spectrometer and the Hamamatsu

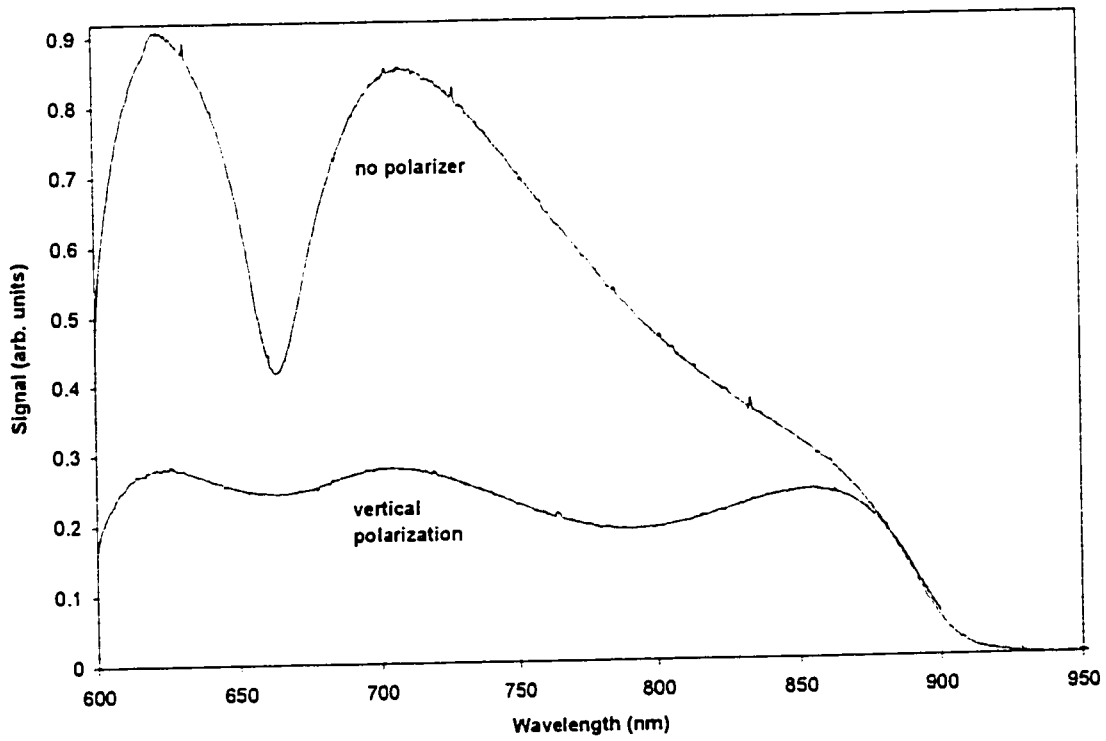

Figure 12 Convolution of Hamamatsu photomultiplier and spectrometer response for vertically polarized light and unpolarized light.

photomultiplier response. From this figure it is clear that the deep valley around 660 nm in the spectrum for unpolarized light is almost completely eliminated in the spectrum for vertically polarized light which also shows much smaller intensity variations. The only disadvantage in detecting only vertically polarized light is that the detected signal is about 3 times smaller than for unpolarized light since the polarizer cuts out half the light and the spectrometer is less efficient for vertically polarized light.

We must also consider another factor in the optical system which can affect the PL spectra. The color filter which is placed before the entrance slit of the spectrometer to cut out the laser light also emits luminescence. The scattered and reflected laser light which reaches the entrance of the spectrometer is sufficient to excite the filter which emits luminescence in the region above its cut-off wavelength. The most often used color filter in our experiments was the Hoya O-56 filter which cuts wavelengths below 560 nm. This filter emitted a nearly constant luminescence from 600 nm to 900 nm which represents the region of interest for the PL from the chromium centers in our crystals.

Fortunately the color filter's luminescence is very weak and is only discernable in the PL spectra when the signal of interest is small. The PL spectra of α-$ZnAl_2S_4$:Cr above room temperature was over a 100 times more intense than the luminescence of the filter. For lower temperatures the PL spectrum from the filter sometimes appeared in the PL spectra of the crystals studied in the region where its luminescence was nearly zero. The only case where the filter's luminescence had a major contribution in the PL spectrum was for PL measurements of the undoped samples of α-$ZnAl_2S_4$ (presented in section 4.6). In the PL spectrum of undoped α-$ZnAl_2S_4$ the emission from the color filter was in the same order of magnitude and needed to be substracted.

3.2.4 PL time-resolved measurements

Time-resolved measurements were realized to study the kinetics of the radiative recombination processes. The setup for the PL time-resolved measurements is illustrated in the lower section of Figure 9 above the acquisition instrumentation. The luminescence decay was investigated under pulsed excitation, provided by the 532 nm line of a frequency doubled Q-switched Nd:YAG laser. The pulse width was $\approx 10^{-8}$ s and the pulse frequency was 10 Hz. The beam was reflected on the crystal near-normal to its surface by a mirror without being first focused by a lens. The rest of the setup is the same as for the steady-state PL experiment except for the acquisition. The time decay of the PL was detected with a RCA: C31034A photomultiplier operating with a high voltage source of 1800 V coupled to the 50 Ω input of a Tektronix 2GS digitizing scope. With this oscilloscope we could register the time evolution of the PL and then transfer the data to a computer. PL spectra were also collected over a time interval of 0.2 ms or 0.3 ms for different time delays between 0.2 ms and 1.2 ms using a PAR Boxcar averager at 78 K and 295 K. This was done to investigate the spectral dependence of the luminescence time decay.

3.3 Optical Gain apparatus

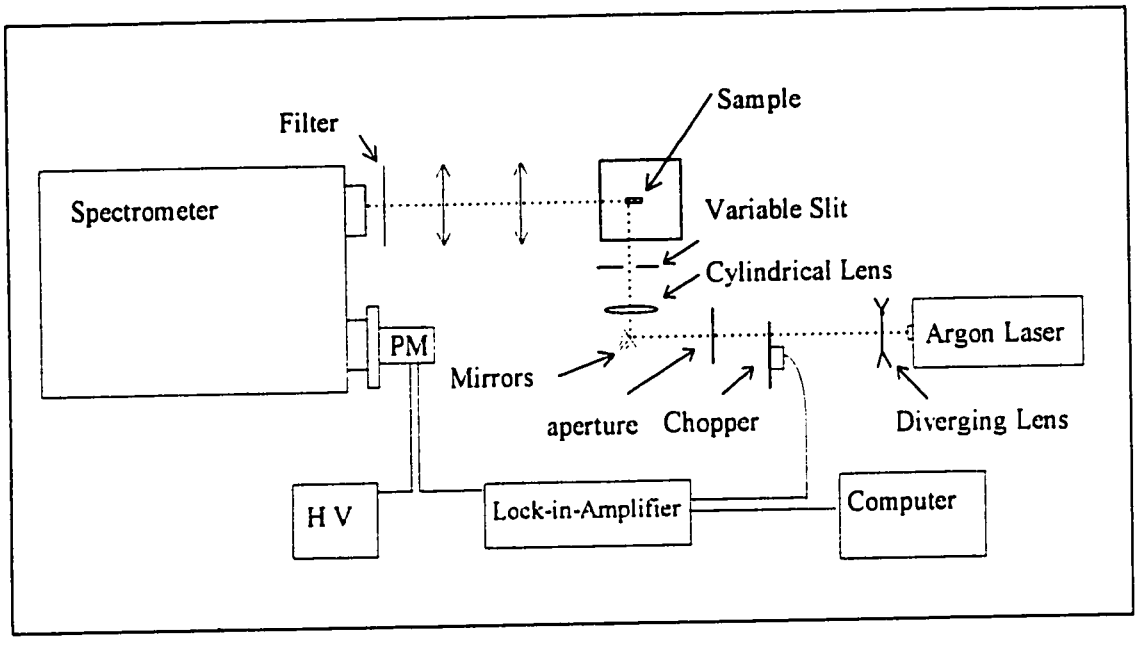

Figure 13. Experimental setup used for optical gain measurements.

To determine the optical gain coefficient we simply measured the emission intensity as a function of the length of excitation on the sample. The complete setup for this experiment is presented in Figure 13 in which the collection and detection schemes are the same as for the PL experiment described in section 3.2.2 except that the luminescence is collected in the 90° geometry. There are also two important additions to the PL apparatus: a cylindrical lens and a variable slit are used to modify the excitation beam. The variable slit is constructed with a digital micrometer and is used to vary the opening between two metal plates. One plate is fixed while the other can be displaced laterally by turning the adjustable screw of the micrometer. The slit length can then be read directly on a digital scale with a precision of 1 μm.

The exciting source came from the argon ion laser used in the multiline mode (488 nm + 514.5 nm) because more intensity is available in this operation mode. Since the laser beam has a gaussian distribution, the intensity decreases rapidly for regions far from the

central maximum. To obtain a uniform intensity beam we must use only the central region. This is achieved by first expanding the beam with a diverging lens (f= 2 m) and then cutting out the edges by passing the beam through an aperture with a diameter of 0.5 cm. The transmitted beam is then passed through the cylindrical lens which focused it into a line on the sample. The variable slit is installed between the cylindrical lens and the sample so that the beam coming from the fixed end of the slit is as close as possible to the side of the sample from which the luminescence is collected. This way the length of the excited region on the sample can be varied easily. At the variable slit the beam is about 5 mm long but less than 2 mm of the central region is used to obtain a uniform beam.

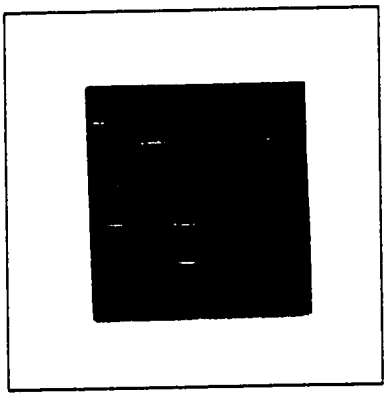

Figure 14 Burn pattern from slit image with magnification ×2

To obtain the magnification of the image from the slit onto the sample, a piece of black photographic paper was placed at the sample position. By illuminating the photographic paper with the transmitted beam from the slit it was possible to obtain the burn pattern of the excitation line for different slit lengths. Figure 14 shows some images of the excitation line for a slit width of 1 mm and 2 mm. By looking at these images through a microscope the length of the image from the slit and the line width can be obtained. The line width must be very narrow since the model used to determine the gain, presented in section 2.6, assumed a unidimensionally illuminated region. The value found for the line width was d= 150 ± 50 μm and the magnification was near unity.

The total intensity of the transmitted beam from the slit was verified to vary linearly with the slit length for values between 0.2 mm and 1.6 mm so this region of slit lengths was used to make gain measurements. The surface of excitation of the sample was good but there were still imperfections present on the surface and in the bulk of the

crystal. This limited the region on the sample which could be used since changes in absorption near these imperfections can cause slight variations in the absolute value of the gain for different positions of the illuminated region on the sample. Furthermore the sample only had dimensions of 2×3 mm which did not leave much room to maneuver around the imperfections.

3.4 Intrinsic PL setup

The intrinsic measurements on α-$ZnAl_2S_4$:Cr were performed in Cagliari, Italy. Figure 15 shows the main components used in the intrinsic experiments. The sample, located in the center of Figure 15, was placed in an optical cryostat model 22C/350C Cryodyne refrigerators which uses helium as refrigerant to obtain a temperature range from 20 K to 300 K. The source of excitation came from a KrF excimer laser which emits pulses of light of 248 nm in wavelength (5 eV). The model of this laser is Lumonics series TE-430-2 operating with 4.78 % (550 torr) of Kr, 0.239 % (110 torr) of F_2 and completed with 2300 torr of He gas. The repetition rate of the light pulses was 5 hz, the pulse

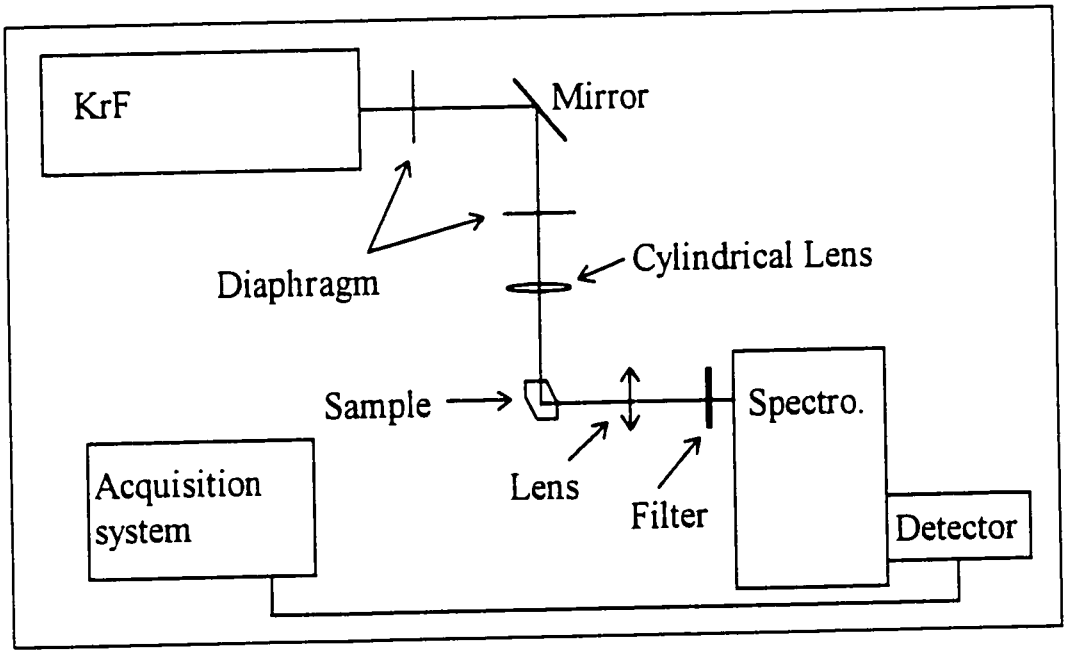

Figure 15 Experimental apparatus for intrinsic measurements

duration was about 7 ns and the excitation intensity was in the order of 13 MW/cm^2. The operation of an excimer laser is based on the fact that in nature some elements exist in the fundamental state only as a monomer, A, whereas in the excited state they also exist in the form of an excimer A_2^*. An excimer is a chemically stable excited state specie that can only exist in the excited state and does not have a corresponding ground state form. An inversion of population can be accomplished between the excimer A_2^* and the fundamental level A when the excimer decays to a dimer which immediately dissociates.

The light beam at the output of the laser has a rectangular shape of 7×20 mm which is passed through a first diaphragm to select the more homogeneous and intense region of the beam. Subsequently the selected region is deviated by a flat dielectric mirror, optimized for the laser wavelength, and after passing through a second diaphragm it is focused by a cylindrical lens on the sample. The light emitted from the crystal is then collected by a lens which focuses it onto the entrance slit of the spectrometer. A filter WG 280 is also placed in front of the entrance slit of the spectrometer to eliminate the excitation light. The spectrometer is an Acton Research Corporation spectra Pro 275 mod. 1235 with a focal length of 27.5 cm and a scanning system. At the output of the spectrometer a detector is used in conjunction with the acquisition system. The detector is a multichannel optical system OMA series III mod. 1420 from EG & G PARC constituted of a system of 512 silicon photodiodes with dimensions of 25 μm × 2.5 mm for a total width of 12.8 mm.

IV-RESULTS AND DISCUSSION

As previously mentioned optical absorption, PL and gain spectra at different temperatures were acquired in order to characterize the α-$ZnAl_2S_4$:Cr crystals. The results obtained from these experiments will be presented and discussed in this chapter. The first part will concern the extrinsic results from the chromium impurities. Absorption measurements were performed in order to find the transition energies involved in the excitation process whereas steady-state PL measurements helped determine the transition energies of the recombination processes. The PL dependence on intensity was investigated and the decay times of the PL were determined over a wide temperature range. Optical gain measurements were done at three different temperatures to verify the potential of this material for laser applications. Finally in the last section the emphasis is put on the host crystal. The results for intrinsic excitation of the chromium doped host are presented along with the extrinsic PL spectrum of the undoped sample.

4.1 Optical absorption spectra

This section presents the results obtained from optical absorption measurements which were realized to investigate the excitation process of the Cr^{3+} ions. The optical absorption spectra of $ZnAl_2S_4$:Cr taken at 295 K and 10 K are presented in Figure 16. The room temperature absorption spectrum consist of two broad bands centered at 2.0 eV (620 nm) and 2.5 eV (495 nm), corresponding to the transitions $^4A_{2g} \rightarrow {}^4T_{2g}$ and $^4A_{2g} \rightarrow {}^4T_{1g}$ of the octahedrally coordinated Cr^{3+} ions (the U- and Y- absorption bands, respectively as defined in section 2.1). The abrupt increase of the absorption in the short wavelength region below 450 nm is due to the band edge of the host crystal since the indirect band gap is around 380 nm as will be shown later in section 4.6. With decreasing temperature a fine structure appears on the long wavelength edge of the U- absorption band (insert Figure 16). These peaks, centered at 1.870, 1.883 and 1.898 eV at 2 K, are ascribed to transitions from the $^4A_{2g}$ state to the $^2T_{2g}$ - triplet orbital.

The energies of the transitions observed in the absorption spectra along with their assignments are summarized in Table 2. From this table we can determine the values of the crystal field parameter, 10 Dq, and the Racah parameter, B, as defined in section 2.1. We obtain 10 Dq= 2.0 eV and from equation (1) B= 0.045 eV. This can be compared to the values for $CdIn_2S_4$:Cr crystals: B= 0.040 eV and 10 Dq= 1.8 eV. The larger value of 10 Dq for $ZnAl_2S_4$:Cr confirms that the crystal field is stronger than in $CdIn_2S_4$:Cr.

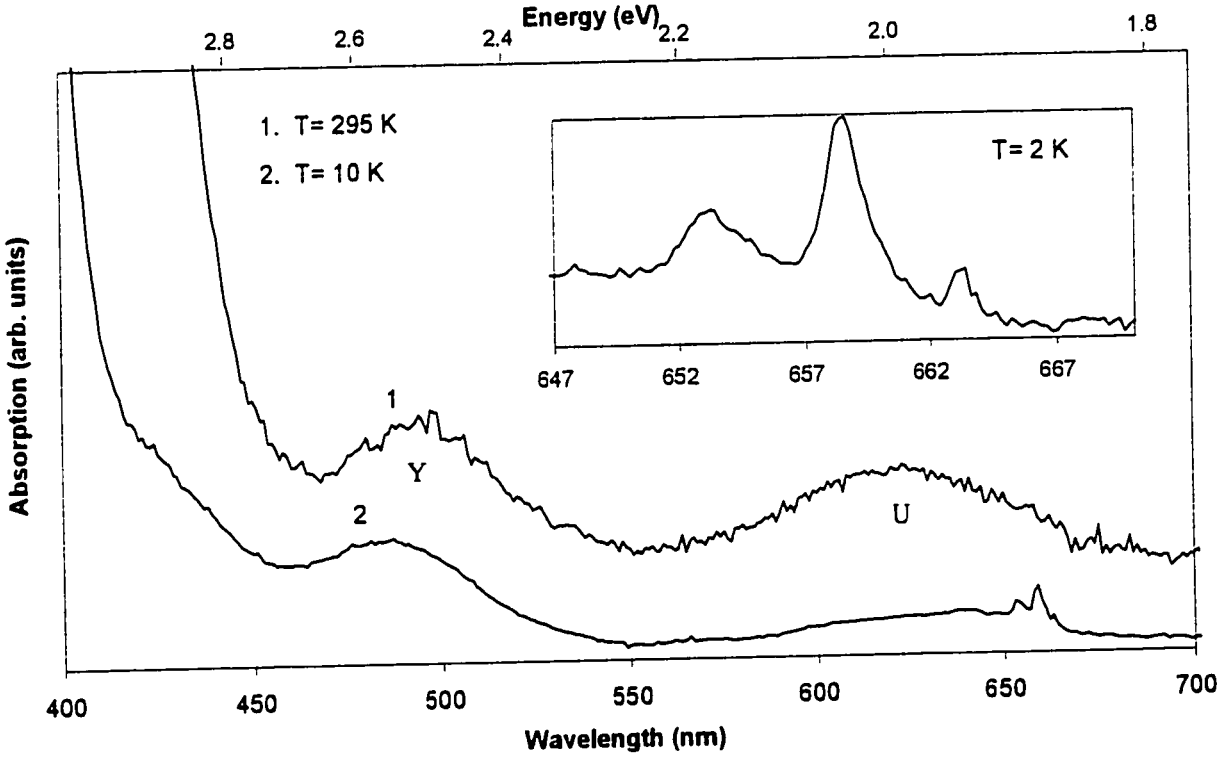

Figure 16 Optical absorption spectra of Cr^{3+} ions in α-$ZnAl_2S_4$ single crystals at 295 K and 10 K. The insert shows an enlargement of the spectral region around the $^2T_{2g}$ triplet at T= 2K.

Table 2 Assignments for Cr^{3+} levels from absorption measurements

ASSIGNEMENT	hν(eV)	T(K)
ABSORPTION		
trigonal crystal field split $\{{}^4A_{2g} \rightarrow {}^2T_{2g}$	1.870 1.883 1.898	2
${}^4A_{2g} \rightarrow {}^4T_{2g}$	2.00	295
${}^4A_{2g} \rightarrow {}^4T_{1g}$	2.50	295

4.2 Extrinsic photoluminescence spectra

The PL experiments were performed in order to investigate the radiative recombination processes in the chromium impurity levels. As explained in section 3.2.2 the PL spectra of α-$ZnAl_2S_4$:Cr was measured in the temperature range 2 K- 530 K and excited with the 514.5 nm line of an argon ion laser. This wavelength was used to obtain excitation into the Y absorption band of the Cr^{3+} ions (Figure 16). This way the electrons are excited from the ground state ${}^4A_{2g}$ to the excited state ${}^4T_{1g}$ and then relax to the radiative states. However for low excitation intensities, the shape of the PL spectra in the near IR region remained unchanged for excitation wavelengths of 248 nm (see section 4.6), and for wavelengths from 488 nm to 620 nm. This indicates the radiative transitions involved in the PL spectrum are independent of the excitation energy above 2 eV, so whatever state the electron is excited to it always relaxes back to the same radiative states. The emission intensity however does depend on the excitation wavelength since the absorption changes.

The steady-state PL spectrum with low intensity excitation at 2 K is presented in Figure 17. At this temperature the spectrum consists of one narrow R_1 zero phonon line (R_1= 771.3 nm) and its vibronic sideband with a fine structure including up to 30 peaks. This R_1 line is associated with the spin forbidden electronic transition ${}^2E_g^{(1)} \rightarrow {}^4A_{2g}$; transition $h\upsilon_1$ in the configuration coordinate diagram (Figure 3). The PL spectra at

higher temperatures are shown in Figure 18. As the temperature is increased to 100 K another R_2 line appears at 765 nm accompanied by anti-Stokes vibronic transitions at wavelengths shorter than the R_1 line. This R_2 line is assigned to the $^2E_g^{(2)} \rightarrow {}^4A_{2g}$ transition based on the Tanabe-Sugano diagram (Figure 2); transition $h\upsilon_2$ in Figure 3. Therefore by increasing the temperature past 100 K, the thermal filling of the R_2 line becomes possible and so the intensity of this emission increases as the intensity of the R_1 line decreases and the intensity of the vibronic sideband saturates. It should be noted that the energy of the R_1 zero-phonon line of $ZnAl_2S_4$:Cr ($h\nu_{R1}$ = 1.609 eV) is practically the same as that of the similar $^2E_g \rightarrow {}^4A_{2g}$ transitions of Cr^{3+} ions in the octahedrally coordinated "ideal" sites of the $CdIn_2S_4$ spinel host [7,22,23].

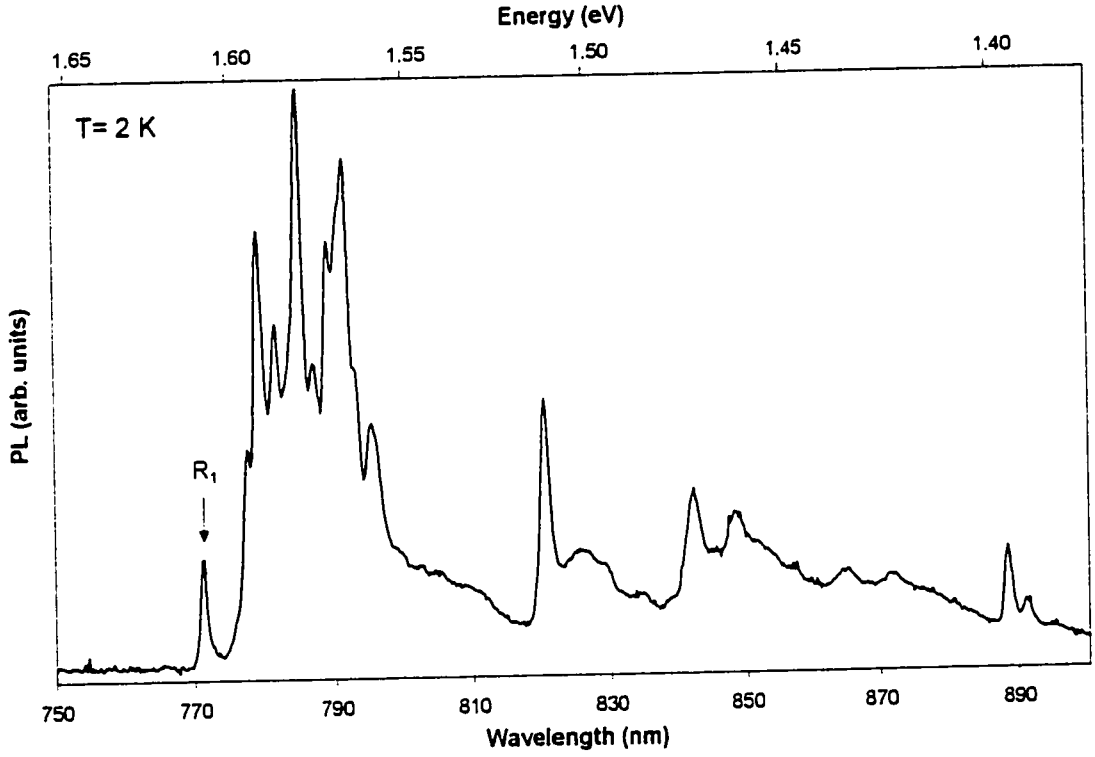

Figure 17 Low intensity extrinsic steady-state PL spectra of chromium ions in α-$ZnAl_2S_4$ single crystals at 2 K displaying the R_1-line and its vibronic sideband.

Further increase of the temperature leads to the gradual broadening and merging of all spectral lines and to the appearance of other components due to the thermal filling of higher excited states of the Cr^{3+} ions. A component of the spin allowed $^4T_{2g} \rightarrow {}^4A_{2g}$ vibronic transitions appears above 300 K at λ~727 nm (U- band); transition $h\upsilon_3$ in Figure 3 of the configuration coordinate diagram. On the opposite end of the spectrum at temperatures above 400 K, the tail of the spectra in the long wavelength region broadens

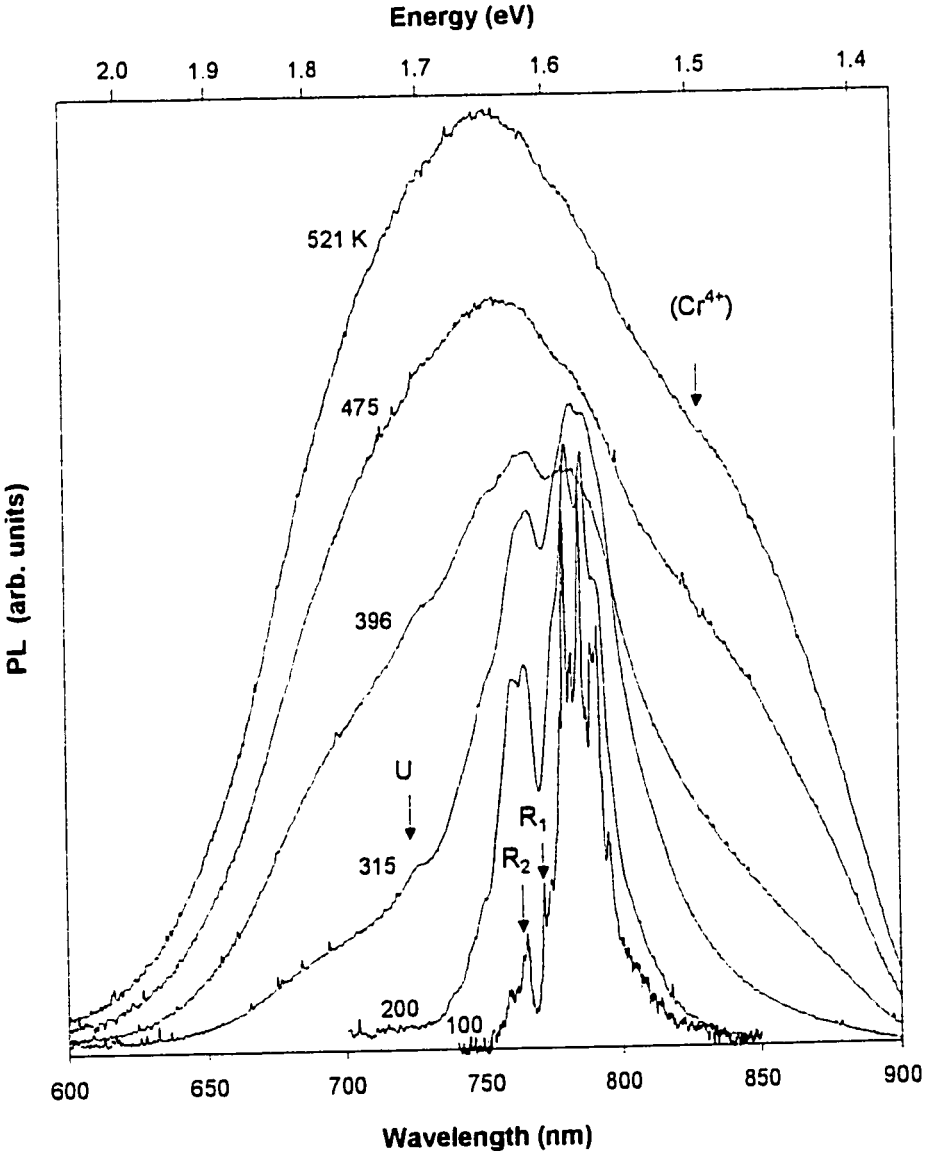

Figure 18 Low intensity extrinsic steady-state PL spectra of chromium ions in α-$ZnAl_2S_4$ single crystals for temperatures from 100 K to 530 K. Spectra at higher temperatures display the gradual broadening of the spectral features. The relative intensities are to scale and the spectra are corrected for the spectral response of detection apparatus.

as a peak seems to develop around 830 nm. This low energy feature can perhaps be attributed to a Cr^{4+} impurity center since the energy levels of these ions are usually located at lower energies than those of Cr^{3+} ions [24,25]. Furthermore the same kind of mixture of Cr^{3+} and Cr^{4+} ions was present in forsterite [24]. L. Kulyuk and S. Popov [19], who supplied us with the samples, also noticed previously that the intensity of this band varied for crystals grown under different preparation conditions. The results from this research were obtained from samples which had a relatively higher Cr^{4+} content, assuming these ions are responsible for the observed band. The speculation that Cr^{4+} ions are present in the crystals is not inconsistent with EPR measurements realized on these samples by G. and A.-M. Lamarche [20].

The values for the energies of the transitions obtained from the PL spectra together with their assignments are inserted in Table 3. From the transition energies presented in Table 2 and 3, the energy differences Δ_1 and Δ_2 (defined in Figure 3) can be determined and are displayed in Table 3. The data from both tables was used to determine the positions of the levels in the configuration coordinate diagram for the Cr^{3+} ions (Figure 3) which was presented in section 2.2.

Table 3 Assignments for Cr^{3+} levels from PL measurements and the energy differences: Δ_1, Δ_2.

ASSIGNEMENT	hν(eV)	T(K)
Δ_1	0.024	
Δ_2	0.246	
EMISSION		
$^2E_g{}^{(1)} \rightarrow {}^4A_{2g}$	1.609	2
$^2E_g{}^{(2)} \rightarrow {}^4A_{2g}$	1.633	260
$^4T_{2g} \rightarrow {}^4A_{2g}$	1.71	535

An interesting feature of this crystal is its increasing overall emission with temperature which could suggest high temperature applications. The integrated near IR emission increases with temperature up to at least 540 K as displayed in Figure 19. For lower temperatures there is a lot of scatter in the data but it can still be observed that the integrated intensity increases slowly with temperature. Actually there is little change in the PL spectrum from 2 K to 30 K. At around 250 K there is a sharp increase in the integrated emission growth rate with temperature. This threshold temperature corresponds to kT= 22 meV which is close to the energy difference between levels $^2E_g^{(1)}$ and $^2E_g^{(2)}$ of the Cr^{3+} ions as shown in Table 3 (Δ_1 as defined in section 2.2). Therefore the onset of thermal excitation of the $^2E_g^{(2)}$ level from the $^2E_g^{(1)}$ level increases the

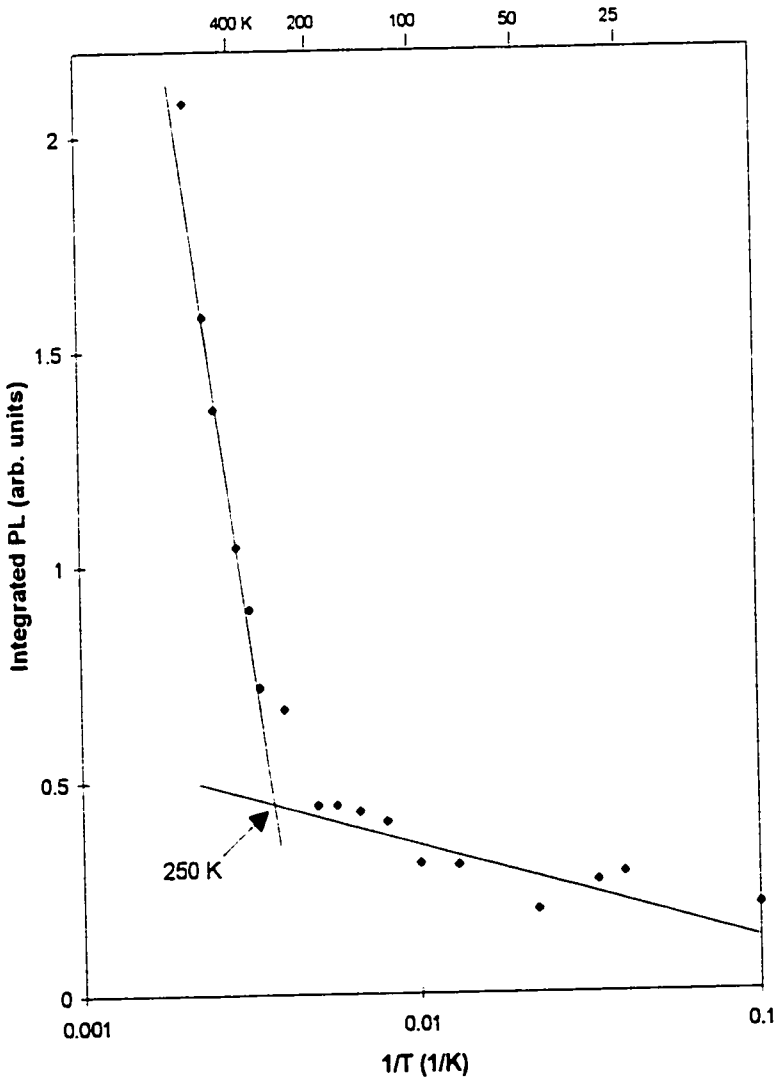

Figure 19 Temperature dependence of the integrated PL in the near IR.

contribution to the total PL emission past the threshold temperature. The continued increase of the emission at relatively high temperatures suggests that the thermal quenching of the luminescence due to radiationless relaxation to the Cr^{3+} ground state is not dominant: on the contrary the luminescence continues to increase up to 540 K because of the thermal filling of higher excited states and possibly of the Cr^{4+} centers.

4.3 PL versus intensity

The PL dependence on the c.w. excitation intensity was investigated in the hope of detecting stimulated emission in $ZnAl_2S_4$:Cr crystals. This stimulated emission would be

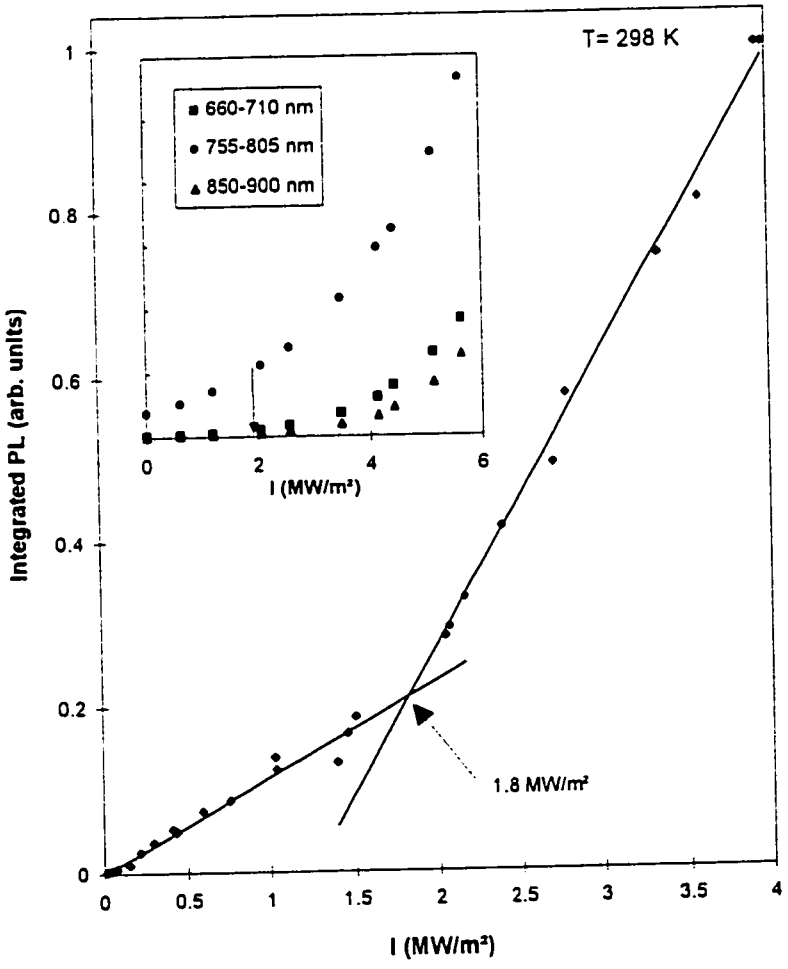

Figure 20 The total near IR emission dependence on excitation intensity at 298 K shows a break at I_c~ 1.8 MW/m^2. Inset: integrated PL for different regions.

characterized by a drastic increase of the measured light output at the point where stimulated emission becomes important. The PL dependence on excitation intensity was realized at two temperatures; 298 K and 528 K. At room temperature (Figure 20) the total emission increases steadily up to a critical excitation intensity of $I_c \approx 1.8$ MW/m^2 where the slope is abruptly augmented. The integrated intensity in three different regions of the PL spectrum (660-710 nm; 755-805 nm; 850-900 nm) is shown in the inset of Figure 20. At I_c the integrated intensity in the wings of the PL spectrum starts to increase steadily whereas under I_c it is nearly zero. This clearly demonstrates that the break in the total integrated PL curve is due to the onset at I_c of contributions from the extremities of the PL spectrum (660-710 nm; 850-900 nm): these are the same spectral regions where optical gain is observed (section 4.5).

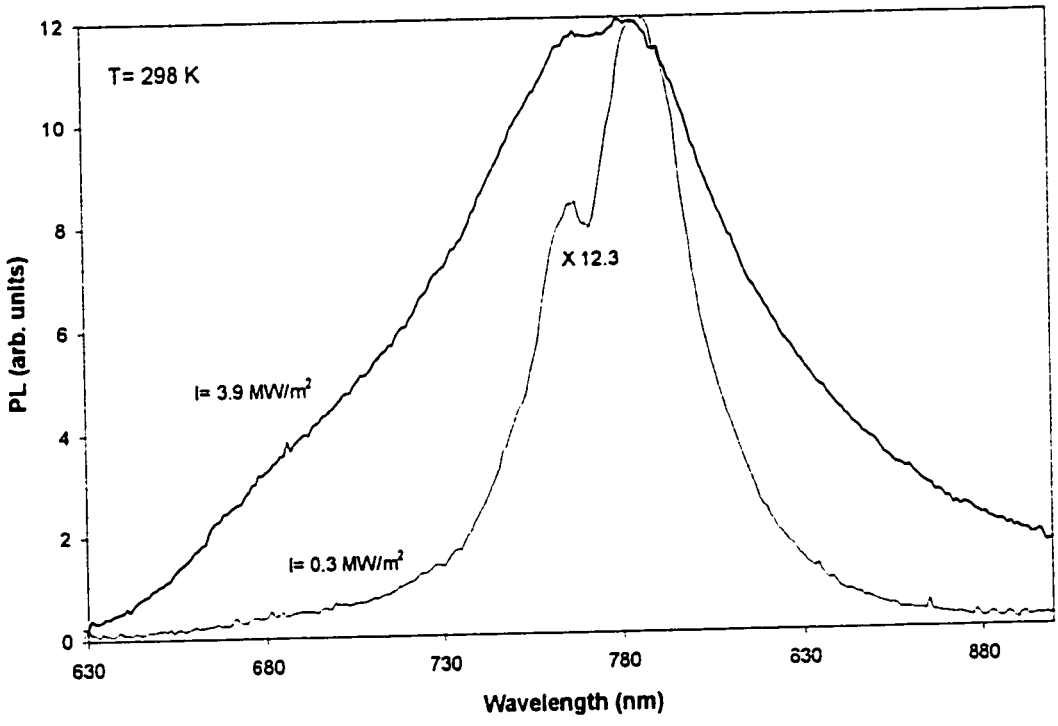

Figure 21 Extrinsic PL spectra at 298 K taken at two excitation intensities, below and above I_c.

The PL spectra at 298 K taken above and below the threshold intensity (I_c) are shown in Figure 21. With increasing intensity the PL spectra broadens as the preeminence shifts from the $^2E_g^{(1)} \rightarrow {}^4A_{2g}$ transition to the $^2E_g^{(2)} \rightarrow {}^4A_{2g}$ transition. Therefore the change

in evolution of the total emission at I_c could be attributed to a saturation of the $^2E_g^{(1)}$ state resulting in the increased filling of the $^2E_g^{(2)}$ state. It is also clear that the contributions from the wings of the PL spectrum are much more substantial at higher intensities.

At 528 K we find again a break in the total emission curve at I_c (Figure 22): however in this instance the total emission is saturated beyond I_c and even seems to decrease. This suggest that all the radiative states of the Cr^{3+} ions are filled past I_c and that non-radiative transitions start to play a greater role at high excitation intensities for this temperature, which would explain the decrease in the total emission. As the excitation intensity is increased above I_c, the spectrum at 528 K, shown in Figure 23, develops a peak around 830 nm which we attributed earlier to a Cr^{4+} center in the host material. The appearance of this peak may find its origin in the continued filling of the Cr^{4+} centers which initiates more transitions in this band as the levels of the Cr^{3+} ions become filled.

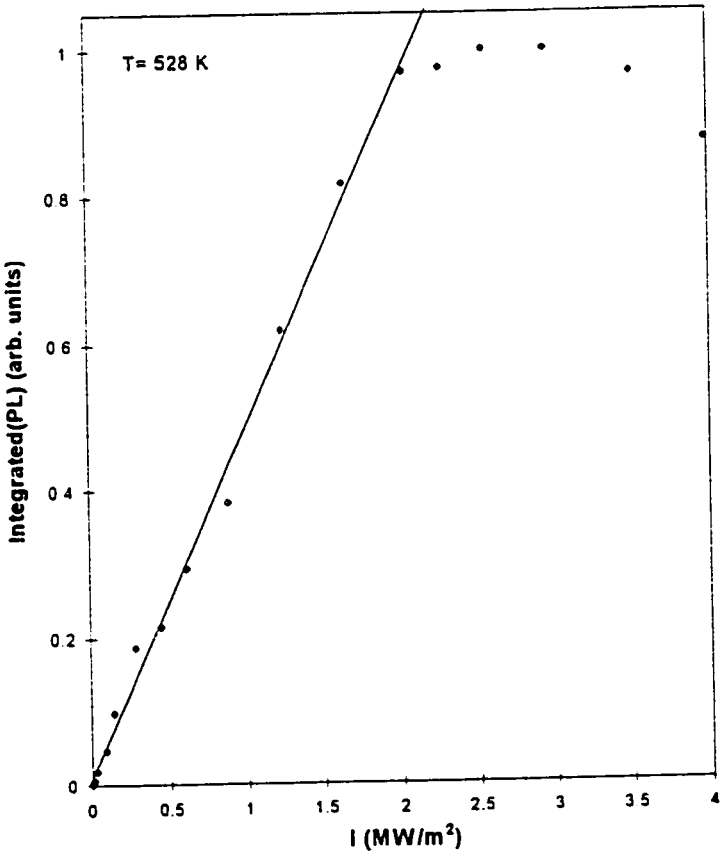

Figure 22 The near IR integrated PL dependence on excitation

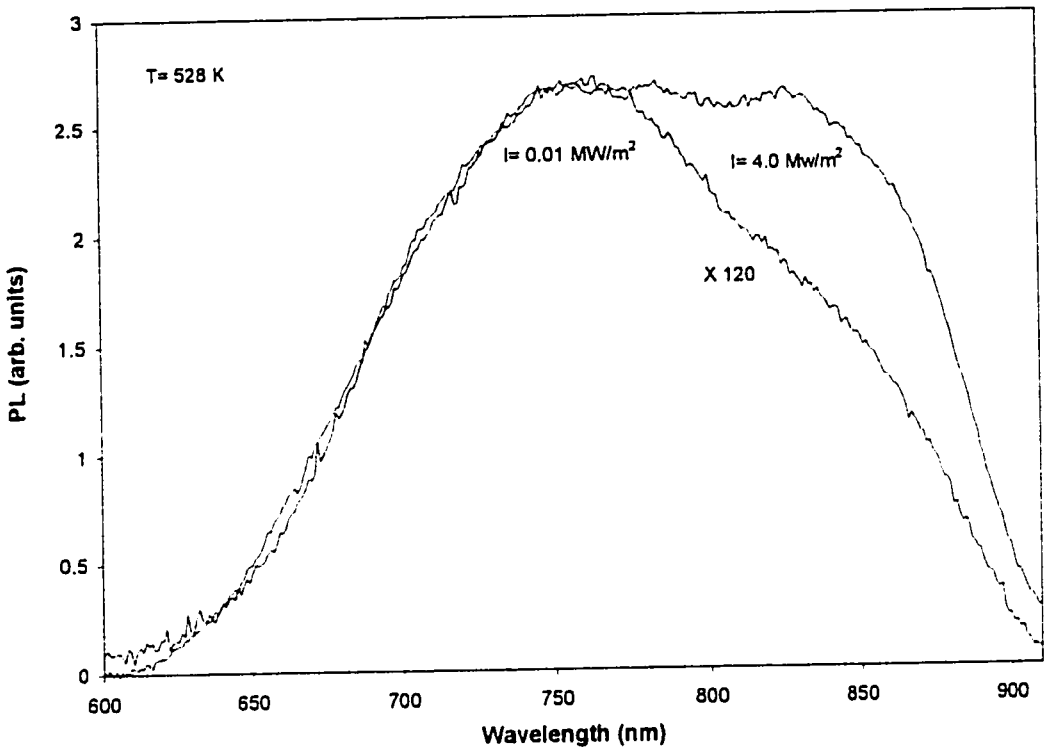

Figure 23 Spectra at 528 K taken at two excitation intensities, below and above I_c.

4.4 Time-resolved measurements

The PL transients provide useful information on the kinetics of recombination. When radiative decay is the only possible decay mechanism, a measurement of the luminescence decay time can provide a direct measure of the radiative lifetime of the excited state of the crystal. However usually the measurement of the luminescence decay time does not provide a direct measurement of the individual radiative lifetimes because of rapid decay via other mechanisms. For the case where nonradiative decay is faster, the measured decay rate is characteristic of the nonradiative processes. In fact the luminescence decay time is the weighted time taken by all the electrons to go back to their ground state, after excitation, by any way available to them. In section 2.4 the kinetic model for a system with four levels was presented, the ground state and the three excited states $^2E_g^{(1)}$, $^2E_g^{(2)}$ and $^4T_{2g}$. The luminescence decay time is therefore a combination of the lifetimes of these states. We assumed the effects of the Cr^{4+} centers were minimal since

the band thought to be due to these centers only appears at high temperatures (T > 300 K) and it is relatively weak for low excitation intensities.

Before determining the luminescence decay times we start by presenting the time dependent PL spectra taken under pulsed excitation at 77 K and 295 K. The results are shown in Figure 24 a) for T= 78 K and b) for 295 K with time intervals for each spectrum of 0.2 ms and 0.3 ms respectively. These spectra were noisier than the steady-state PL spectra because the time integrated luminescence intensity induced by pulsed excitation was about a 1000 times weaker. Therefore the time-resolved curves had to be averaged but they still retained the same form as the steady-state curves. If we look at the time evolution of the PL spectra at 295 K (Figure 24 (a)), their shape does not show any appreciable variation in time other than a decrease in intensity. The same behavior is observed in the spectra at 78 K (Figure 24 (b)) and was verified for spectra taken between 10 K to 300 K. Therefore at least between 10 K and 300 K all spectral components displayed the same time constant, indicating a dominant emission process at each temperature.

Figure 25 shows the experimental temperature dependence of the extrinsic luminescence decay time $\tau(T)$ obtained from low intensity pulsed excitation. The luminescence decay time, τ (points on Figure 25 (b)), is the time taken for the emission intensity to decrease by a factor 1/e from the maximum so τ was calculated by fitting the exponential decay curves with an equation of the form $Ae^{-t/\tau}$ where t is the time and A a constant. The natural logarithm of the PL intensity is plotted as a function of time in Figure 25 (a) for a temperature of 298 K. This linear dependence indicates the temporal decay is exponential, which was the case at all temperatures (2-540K). Distinct lifetimes could not be separately measured at a given temperature because of the large overlap between the different bands.

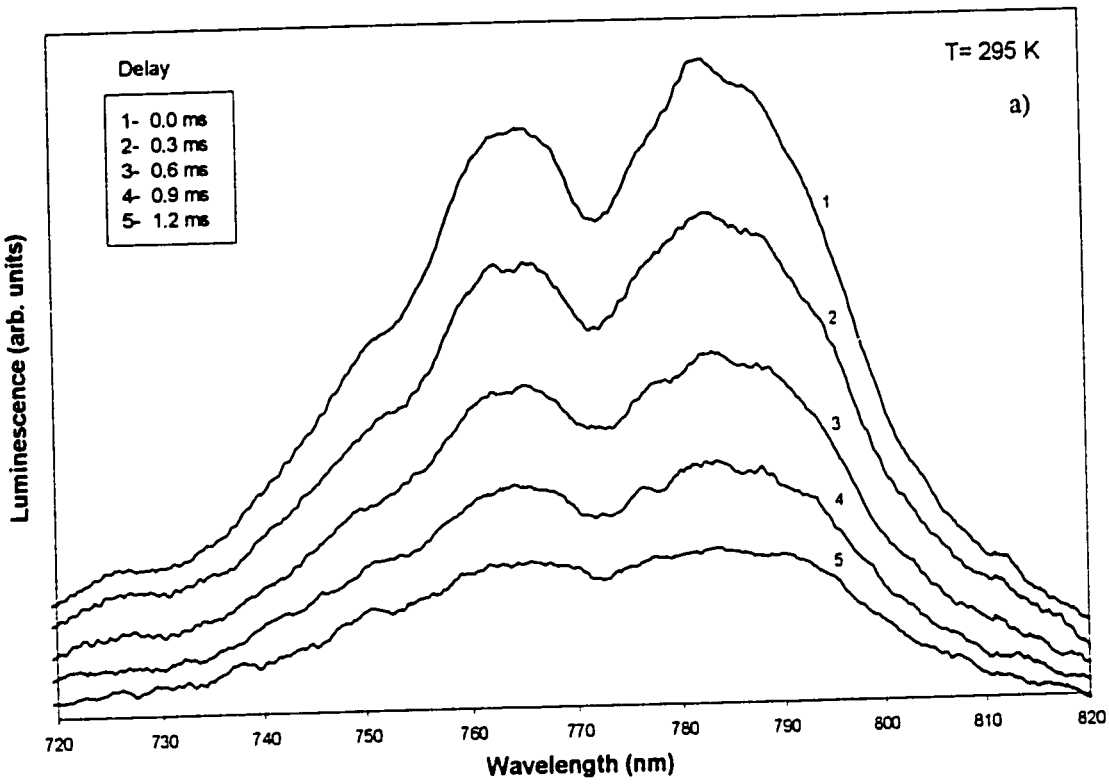

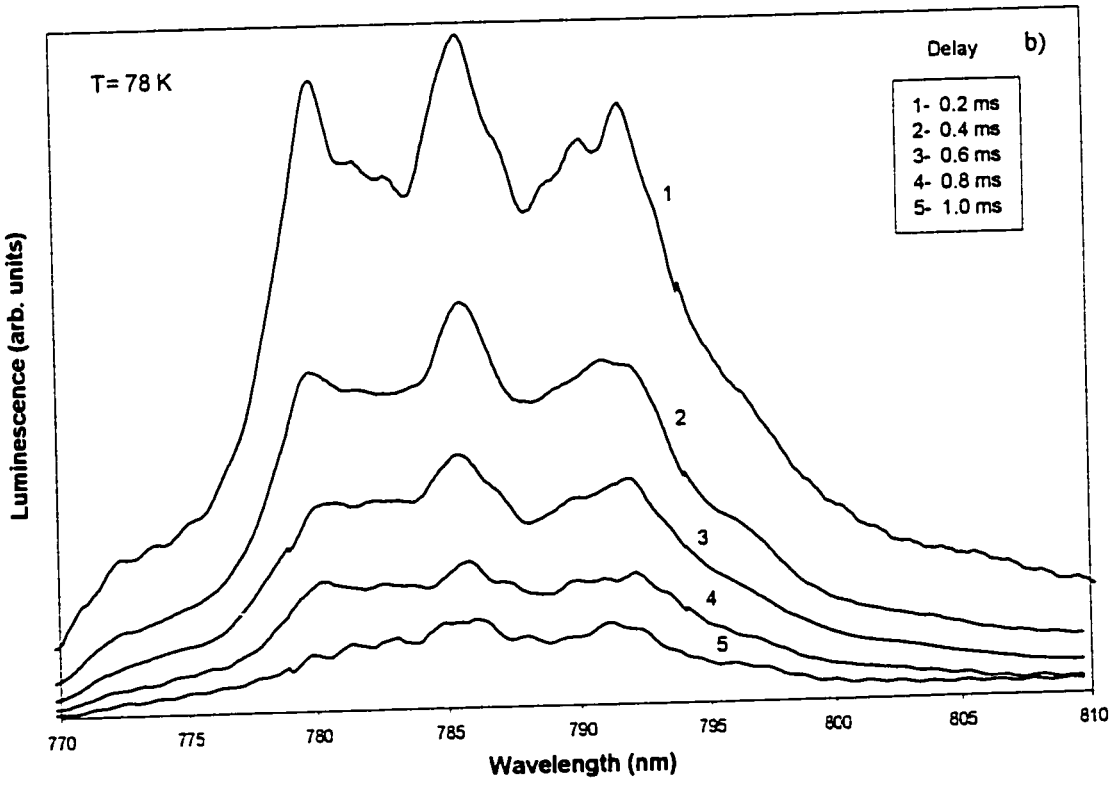

Figure 24 PL spectra under pulsed excitation for different time delays at a) T=295 K and b) T=78 K

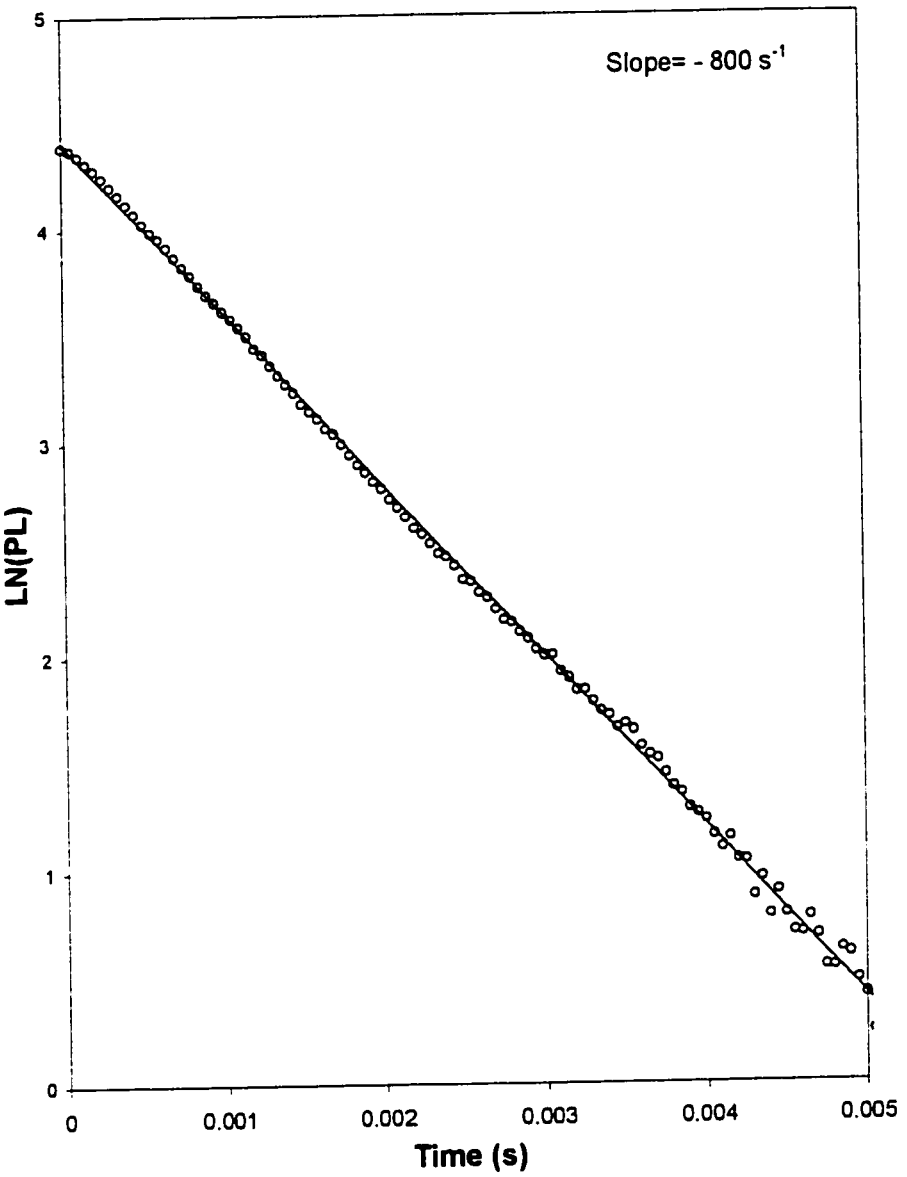

Figure25 a) Dependence in time of the natural logarithm of the photoluminescence intensity taken at 298 K. This linear dependence implies and exponential decay with time of the luminescence. The slope corresponds to $-1/\tau$ so the time decay at this temperature is 1.25 ms.

At low temperatures it was observed from the PL spectra (Figure 17-18) that the Cr^{3+} lifetime is dominated by the $^2E_g^{(1)} \rightarrow {}^4A_{2g}$ transition. Also since the thermal energy available at 2 K is negligible, the nonradiative transitions are minimal and the lifetime of state $^2E_g^{(1)}$ can be measured directly so $\tau_{E1} = \tau(2K) = 4.7$ ms. As the temperature is increased further a higher percentage of the excited Cr^{3+} ions will be in the shorter lifetime $^2E_g^{(2)}$ and $^4T_{2g}$ states because of thermal excitation and consequently more transitions from

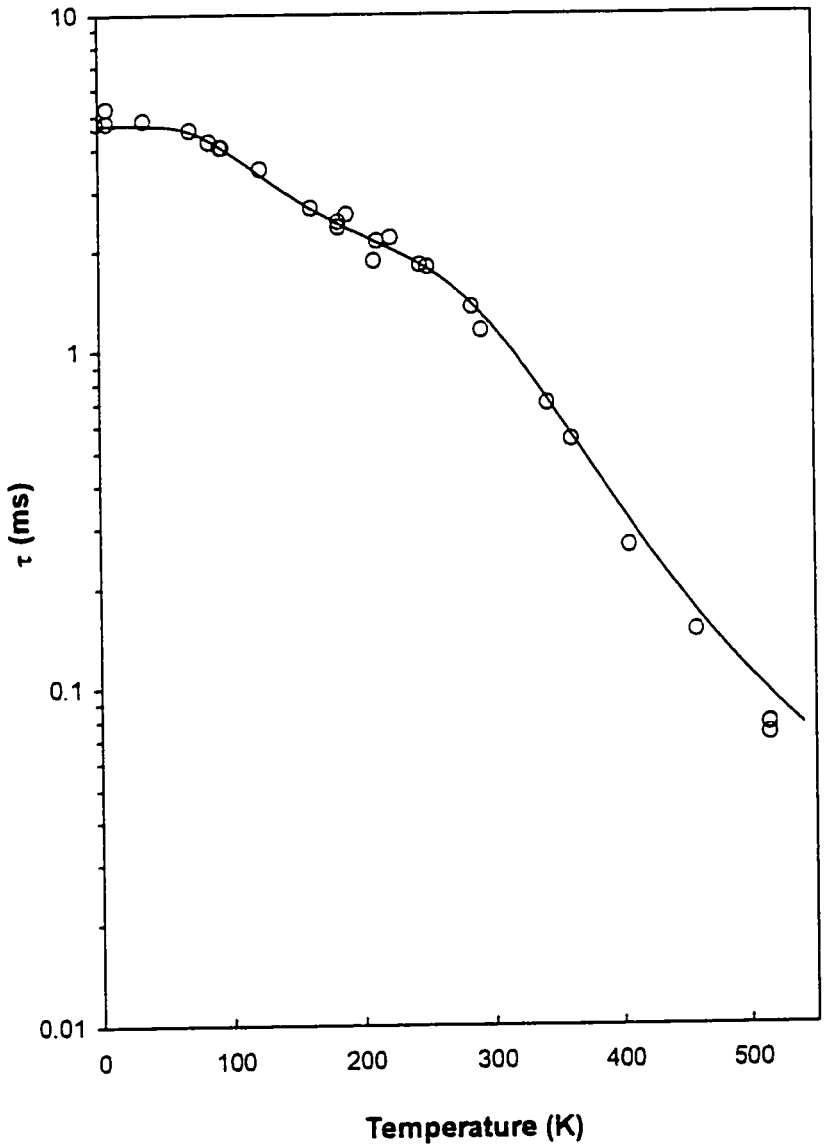

Figure 25 b) PL decay time from 2 K to 537 K. Solid line represents fit to equ. (5)

these states will be initiated resulting in a decrease of τ. A plateau at τ_E is observed up to about 70 K where the luminescence decay time begins to decrease steadily. This temperature corresponds to the onset of luminescence from the $^2E_g^{(2)} \rightarrow {}^4A_{2g}$ transition in the PL spectrum. Again at 300 K there is a change in the time decay curve as τ decreases more rapidly. From figure 18 we note that this temperature corresponds to the onset of luminescence coming from the $^4T_{2g}$ state.

In order to describe the temperature dependence of the PL decay, equation (5) obtained from the kinetic model presented in section 2.4 is fitted to the experimental luminescence decay times. The values for the lifetimes of the excited levels and the Δ_1, Δ_2 energy differences, obtained from the fit of the $\tau(T)$ dependence over the whole temperature range (solid line on Figure 25) are τ_{E2}= 0.55 ms, and τ_{T2}= 1.9 μs; Δ_1=0.03 eV, Δ_2=0.24 eV. The energies of the Δ_1 and Δ_2 gaps, obtained independently from the optical absorption and steady-state PL spectra (shown in Table 3) and from the temporal measurements are very close.

To acquire additional information concerning the recombination processes, the decay time was also measured as a function of the excitation intensity. Former observation of gain in $CdIn_2S_4$ [26] was accompanied by a sudden drop in the PL decay time at a critical excitation intensity which characterized the onset of stimulated emission so it is hoped the same behavior will occur in $ZnAl_2S_4$:Cr. The intensity dependence of the decay time taken at 725 nm at room temperature is shown in Figure 26. The decay time was determined under low intensity pulsed excitation at 532 nm while the intensity of a continuous background excitation (514 nm) was varied. The decay time remains fairly constant up to an intensity I_c where τ starts to decrease abruptly. Here again I_c~ 2 MW/m^2 is very close to the previously found value taken from the break in the total emission dependence on intensity (Figure 20). As indicated earlier, the long lifetime R_1-line is saturated past a critical intensity. Therefore the decay time decreases and the PL

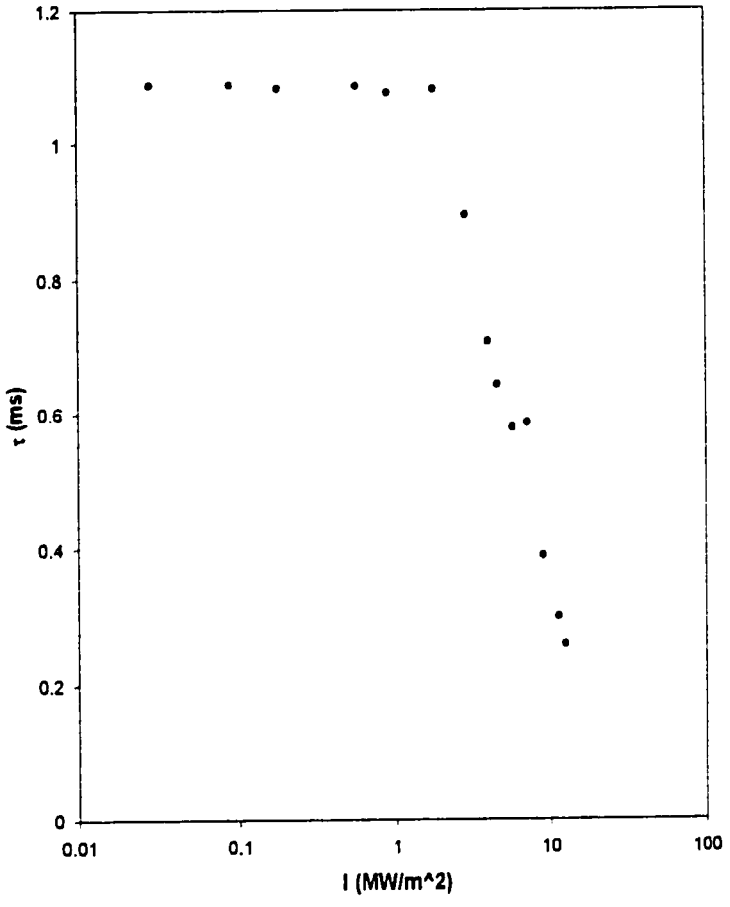

Figure 26 The intensity dependence of the Cr^{3+} lifetimes; τ remains constant up to I_c~2 MW/m^2 after which it decreases rapidly.

increases as the shorter lifetime $^2E_g^{(2)} \rightarrow {}^4A_{2g}$ transition starts to dominate the Cr^{3+} luminescence.

4.5 Gain measurements

The observation of a change in behavior of the PL past a critical excitation intensity could indicate the condition for stimulated emission and thus optical gain. The net optical gain (g) due to stimulated emission is extracted from I_l, the PL at 90° from the incident beam, by fitting the data to equation (9). Figure 27 shows a sample of the data used to calculate the gain values for various wavelengths at 298 K. The points in the figure represent the experimental values and the solid lines are the fits from equation (9).

The dashed line represents the Rayleigh scattered light from the exciting laser (514 nm) for different *l* values.

For an excitation energy below I_{th}~2 MW/m^2 no gain was found but stimulated emission was observed above this threshold intensity. This is shown on Figure 28 where gain values taken at 750 nm are plotted for different excitation intensities. The threshold intensity were the onset of population inversion arises is close to the previously established critical intensity for the PL emission and decay times. In Figure 29, the gain spectrum at 298 K is shown for an excitation intensity above and below I_c. For an excitation intensity

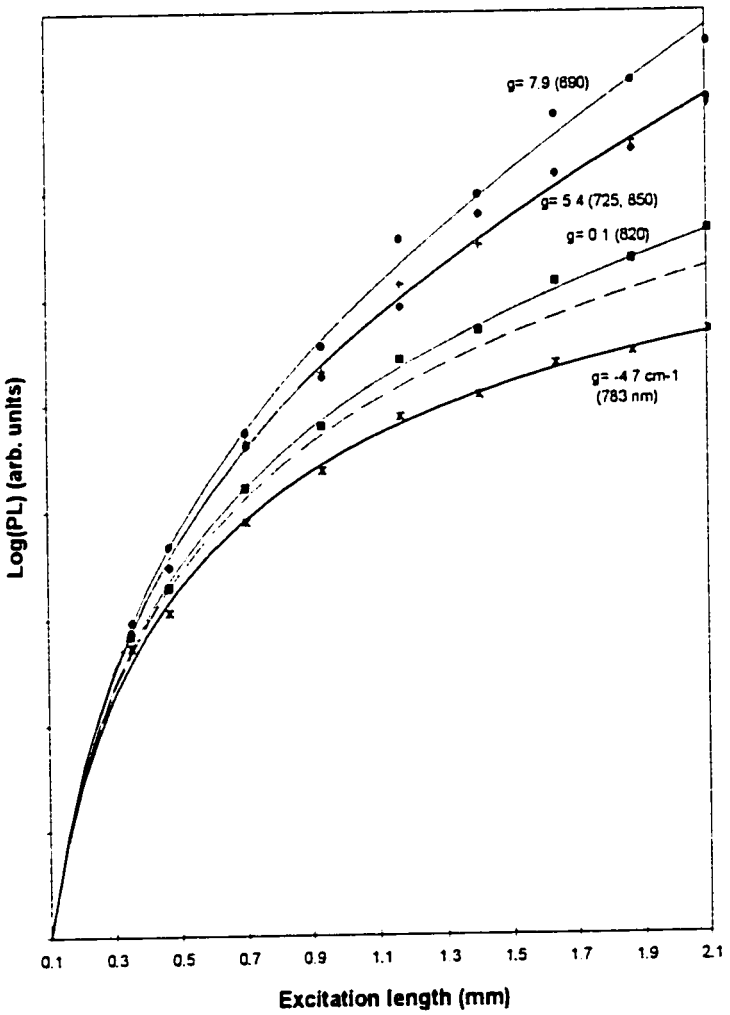

Figure 27 Logarithm of the PL intensity for different excitation lengths on the sample taken at 295 K with I= 4.2 MW/m^2. The points are the experimental values and the solid lines are fits. The dashed line represents the Rayleigh scattered light from the exciting laser.

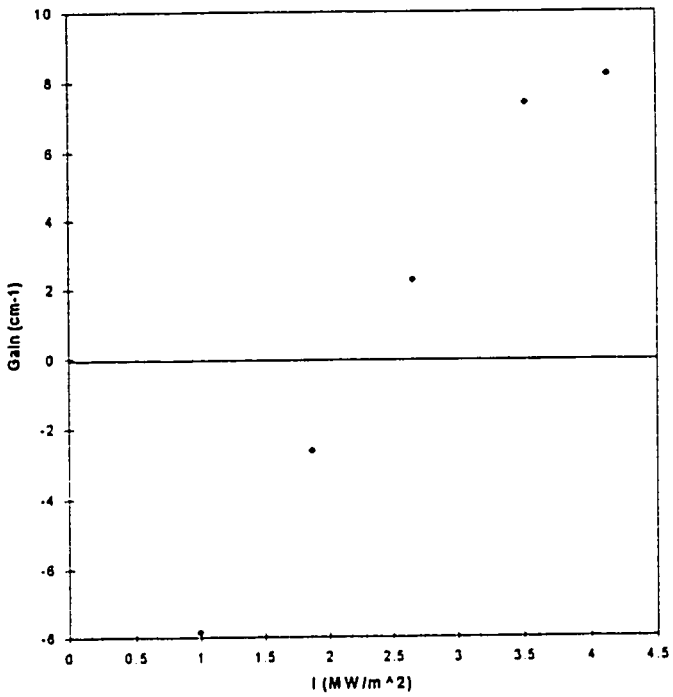

Figure 28 Gain values taken at 750 nm for T= 298 K for different excitation intensities.

of 0.3 MW/m^2 (Figure 29 (b)) only absorption is present. For an excitation intensity of 4.1 MW/m^2 (Figure 29 (a)) no gain is found at the PL peak around 783 nm! On the contrary the gain is observed in the wings of the PL spectrum around 700 nm and 850 nm with maximum values around 9 cm^{-1}. The gain values had uncertainties up to ±1 cm^{-1}.

The gain spectrum at 198 K is presented in Figure 30 and displays gain values up to 22 cm^{-1} at 730 nm. The spectral range of the data was not extended far enough which is why the gain values at the extremities of the spectrum seem to continue rising. Also the values at the extremities of the spectrum are less reliable since the PL emission in this region was weak and therefore the signal was noisier. At higher temperatures, the gain in the band around 700 nm decreased until absorption started to dominate. However at 380 K there was still some gain observed in the long wavelength side of the spectrum with values up to 6 cm^{-1} at 890 nm.

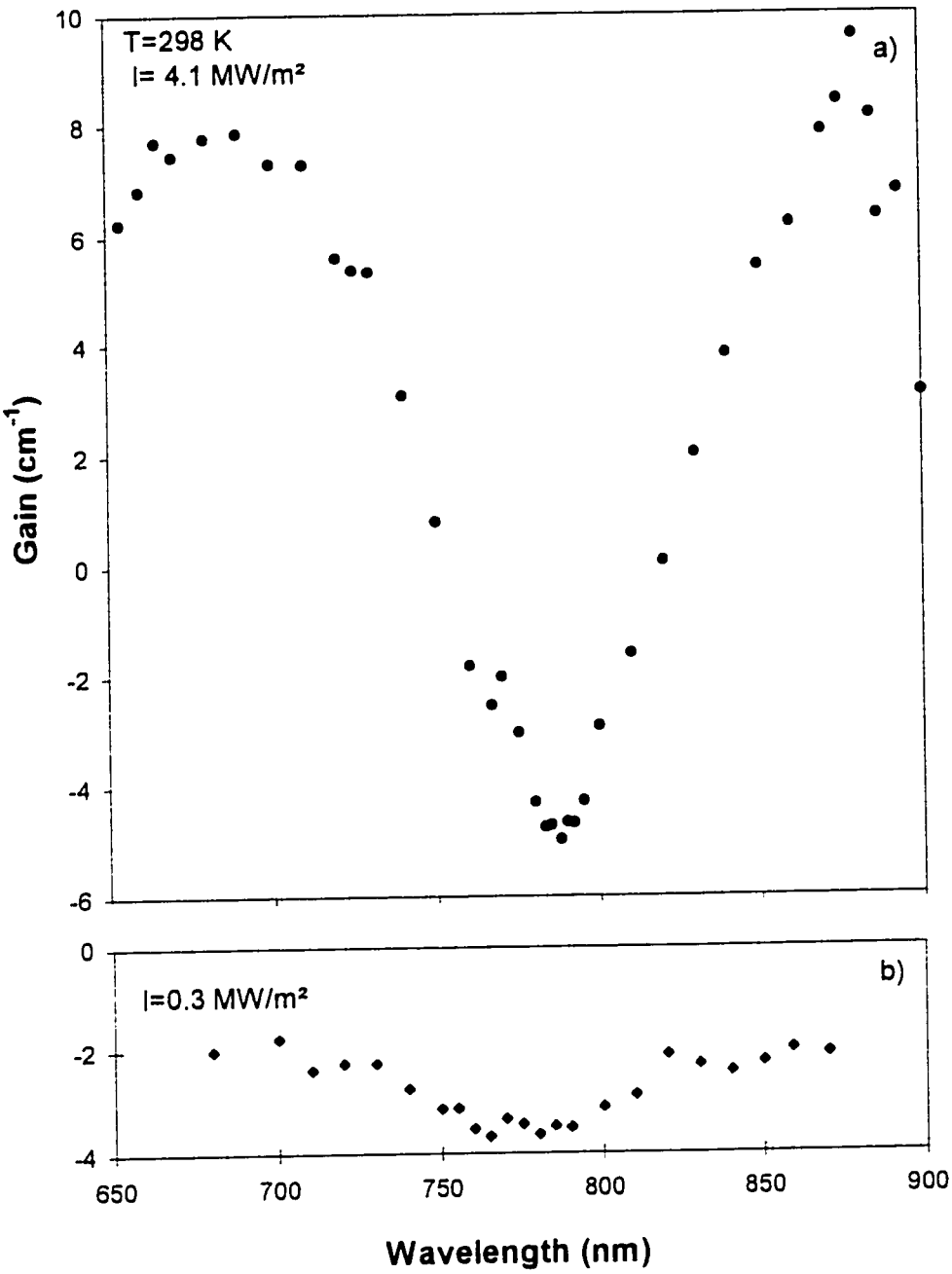

Figure 29 Gain spectrum of α-$ZnAl_2S_4$:Cr at 298 K with an excitation intensity of a) 4.1 MW/m² and b) 0.3 MW/m².

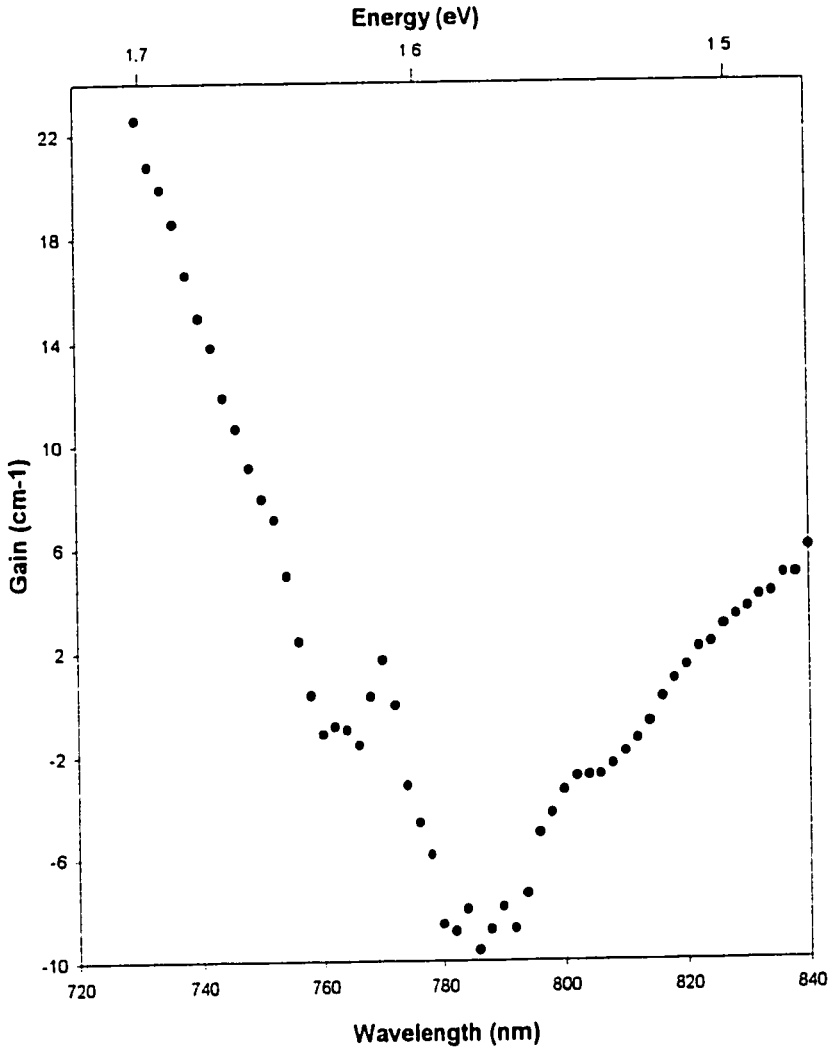

Figure 30 Gain spectrum at 198 K for an excitation intensity of 4.1 MW/m^2.

Therefore from gain measurements we find that stimulated emission occurs in the region of the short lived $^4T_{2g} \rightarrow {}^4A_{2g}$ transition ($\lambda \sim$ 730 nm) and possibly of the Cr^{4+} centers ($\lambda \sim$ 830 nm). Consequently the optical gain due to the transition $^4T_{2g} \rightarrow {}^4A_{2g}$ can be attributed to a four-level system with the fourth level being a virtual vibronic state similar to the alexandrite laser as presented is section 2.5. Figure 6 showed the four-level laser energy-level diagram where the ground level is $^4A_{2g}$ and the upper laser level is $^4T_{2g}$. As for the mechanism responsible for the stimulated emission from the Cr^{4+} centers, it cannot

be determined until the energy levels involved are found. Therefore further measurements in the near IR past 900 nm would be useful to locate the Cr^{4+} energy levels. However this implies the use of a germanium or InGaAs based photodetector which is less sensitive than the photomultiplier we used, making the measurements above 900 nm more difficult.

4.6 Photoluminescence of host crystal

Extrinsic PL measurements on undoped α-$ZnAl_2S_4$ crystals were realized in part to determine if the band, appearing around 830 nm at high temperatures or high excitation intensities in the near IR PL spectra, could be due to a defect center in the host crystal as opposed to Cr^{4+} ions as suggested in section 4.2. There is poor agreement between previous reports of PL measurements in undoped α-$ZnAl_2S_4$ crystals [1,2]. The PL in α-$ZnAl_2S_4$ crystals studied by Kai et al. [2] showed a broad green emission at 540 nm at low

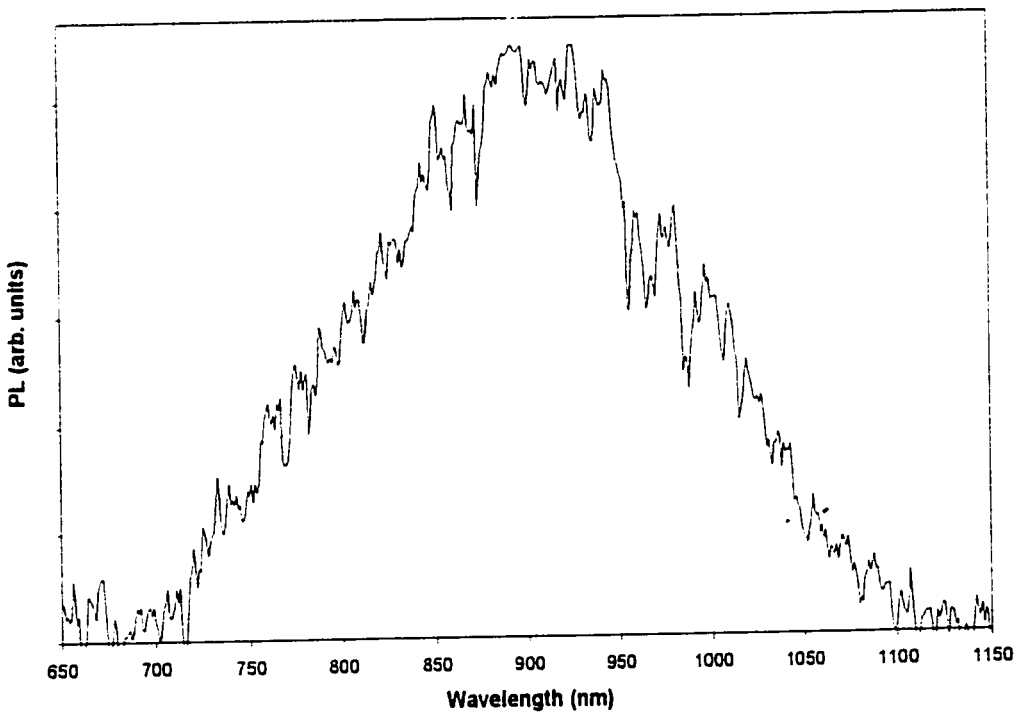

Figure 31 Extrinsic PL spectrum of undoped α-$ZnAl_2S_4$ crystals at 298K.

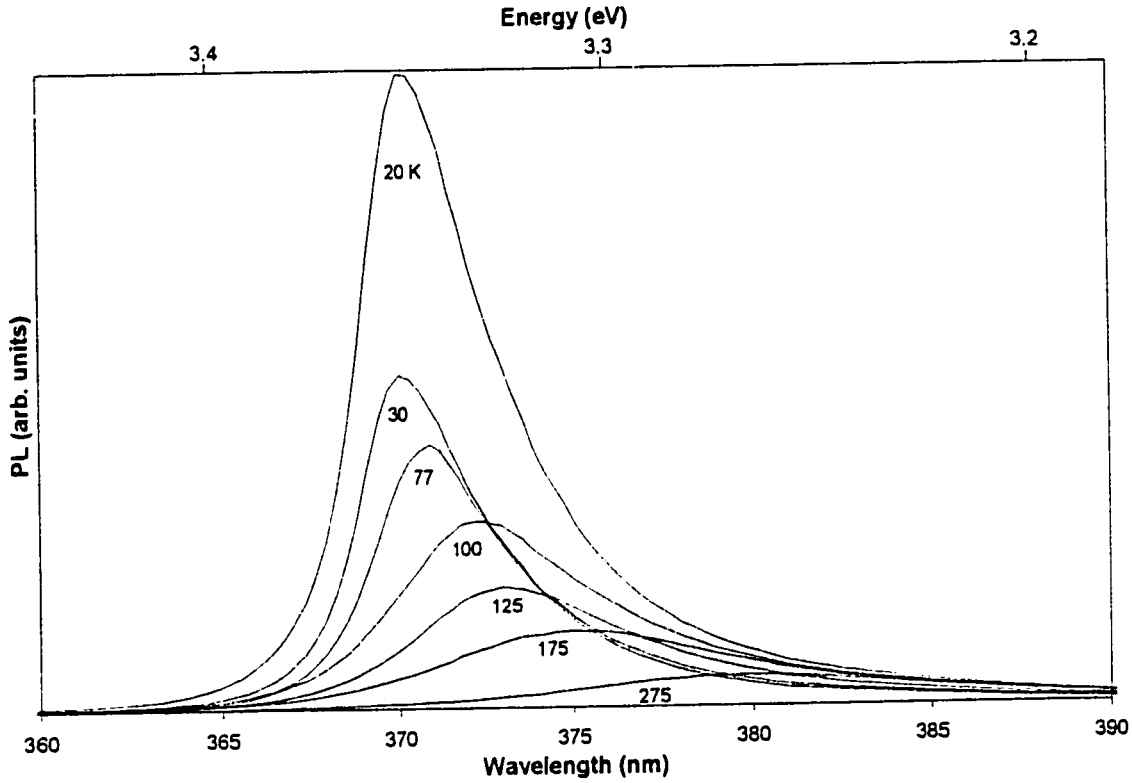

Figure 32 Intrinsic PL spectra of α-$ZnAl_2S_4$:Cr at various temperatures under pulsed UV excitation.

temperatures and a weak near IR emission at room temperature consisting of two bands at 790 nm and 850 nm. Conversely the paper by Kulikova et al. [1] reported two broad bands at 450 nm and 600 nm.

Our PL measurements on undoped α-$ZnAl_2S_4$ taken with an extrinsic excitation of 514.5 nm, displayed one weak band at 905 nm at 298 K as shown in Figure 31. The spectrum is very noisy since the signal obtained was very weak. The Si detector used to obtain a spectral response further in the IR was less efficient than the photomultiplier usually used and this PL band was at least 100 times weaker than the near IR emission at this temperature in Chromium doped samples (Figure 18). In our results and those by Kai et al. [2] there was an IR band around 905 nm, and 850 nm respectively in the undoped crystals but it was much too weak to explain the extrinsic PL band found around 830 nm or the gain observed in this region in the chromium doped crystals.

PL intrinsic measurements were also realized on α-$ZnAl_2S_4$:Cr. The PL spectra obtained under pulsed excitation in the UV region (5 eV) showed one strong peak in the UV, shown in Figure 32 for different temperatures, and a broad band about 200 times less intense in the near IR. In the previous reports [1, 2] on undoped α-$ZnAl_2S_4$, no peak was seen in the UV but this might be due to the smaller excitation energy used (3.8 eV as compared to 5eV here). Furthermore the green bands observed in [2] would be masked by the tail of the UV emission in our spectra. As for the longer wavelengths (not shown in Figure 32) the band in the near IR associated with the chromium impurity center, which is described in section 4.2, was seen here as well.

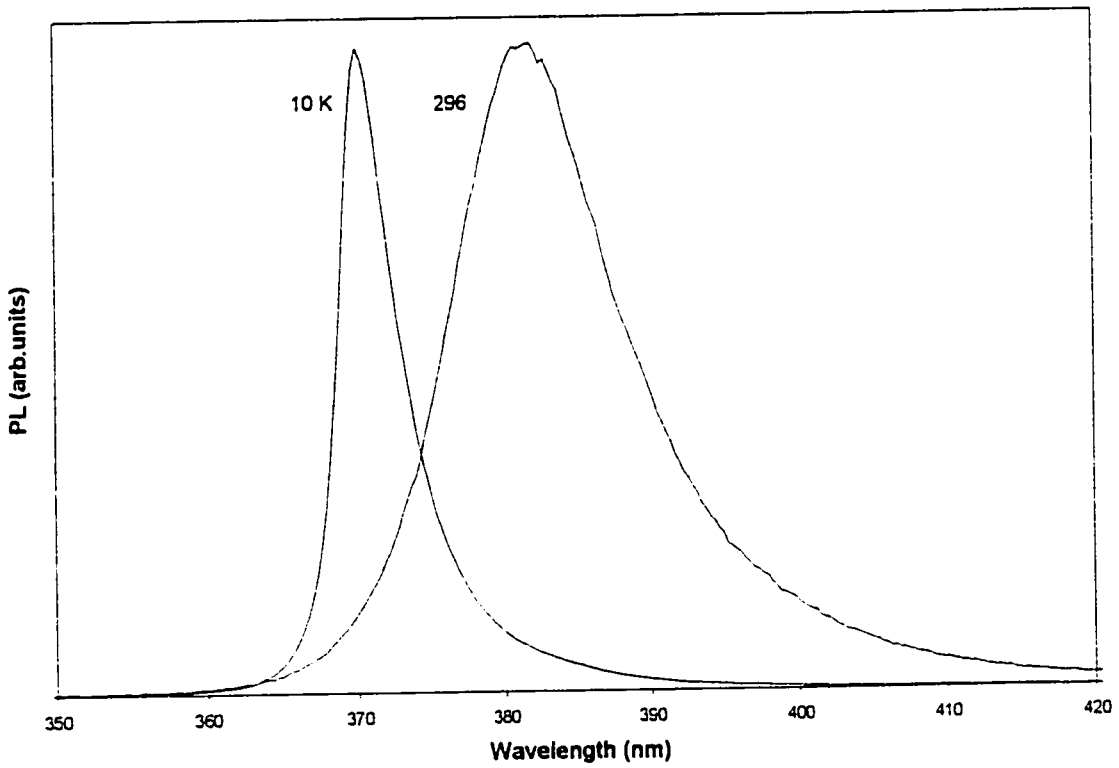

Figure 33 Intrinsic PL spectra of α-$ZnAl_2S_4$ at 10 K and 298 K. Relative intensities are not to scale.

The peak in the UV is displaced from 370 nm at 10 K to 381 nm at 296 K; it is therefore located at energies very close to previously reported values of the indirect band

gap of α-$ZnAl_2S_4$ (3.42 eV (362 nm) at 300 K [3]). Figure 33 shows the UV spectrum at 10 K and a magnification of the spectrum at 296 K. At low temperatures the peak is narrow and non-symmetric extending further into the long wavelengths. As the temperature is increased the PL intensity decreases rapidly (Figure 32) and the spectrum broadens with the long wavelength tail extending up to 600 nm at 296 K. This suggests there are more transitions assisted by phonon emission at low temperatures; as the temperature is raised to 300 K there is more phonon assisted transitions and phonon absorption starts to play a greater role.

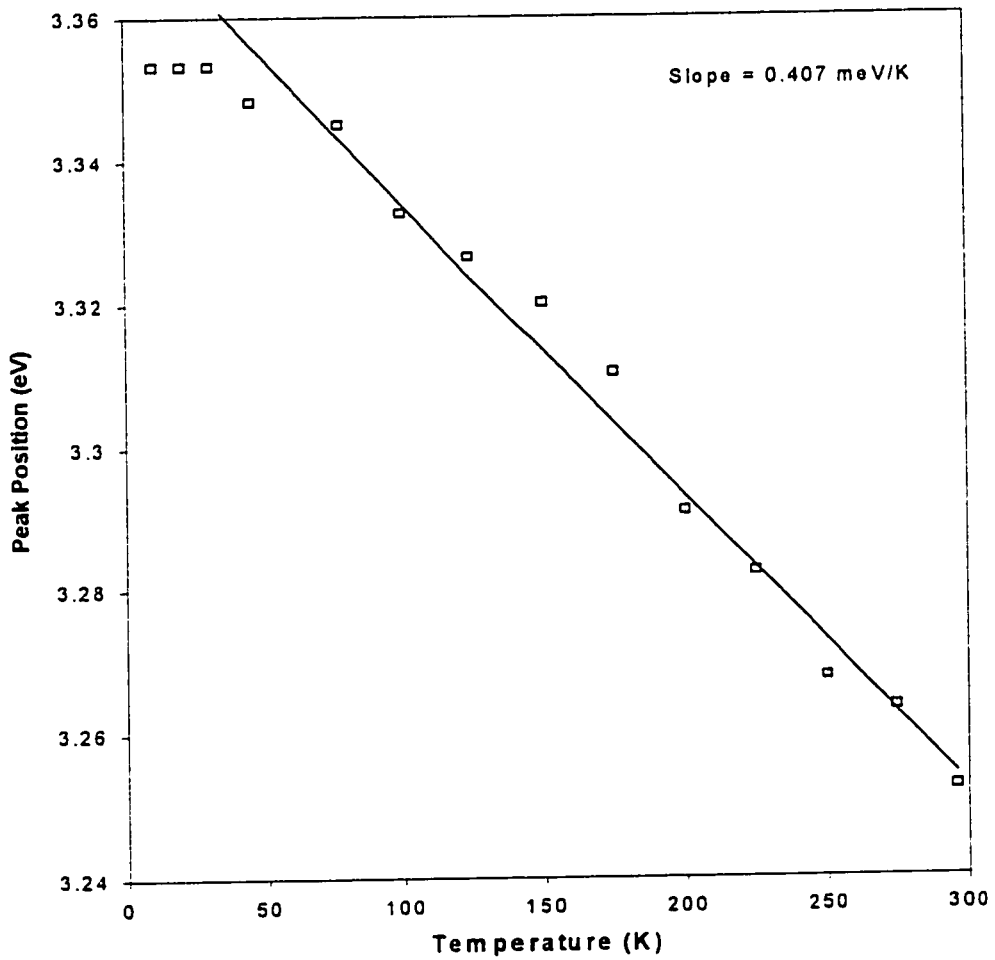

Figure 34 Temperature dependence of the peak position of the intrinsic PL spectra of α-$ZnAl_2S_4$.

The temperature dependence of the peak position is shown in Figure 34. From 10 K up to 40 K the peak position remains nearly constant around 3.35 eV. Upon further increase of the temperature its position starts to decrease linearly at the rate of 0.407 meV/K up to 300 K. This energy variation is comparable to that of the energy gap of $CdIn_2S_4$ in the same range [27]. The half width half maximum (HWHM) of the peak remains constant at 0.04 eV up to 80 K after which it increases up to 300 K where HWHM= 0.12 eV. The fast time decay of the peak, τ= 25 ns, remains constant at all temperatures indicating there is only one component contributing to the emission. Since the excitation energy (5eV) is higher than the direct band gap (4.4 eV [3]) we assume the emission process takes place via excitation of the direct band gap followed by relaxation to the indirect band gap and UV emission. Furthermore the temperature behavior of the UV emission is consistent with that of a band edge suggesting the peak position (Figure 32) represents the indirect band gap of α-$ZnAl_2S_4$ in the 10-300 K range.

V- CONCLUSION

The present research was undertaken in order to study the optical properties of chromium doped α-$ZnAl_2S_4$ by absorption, PL and optical gain measurements. The PL and absorption spectra, at low light intensities, were obtained for different temperatures and yielded the energies of the Cr^{3+} impurity levels. Also the appearance at high temperatures of a band around 830 nm was attributed to Cr^{4+} impurity centers. The spectroscopic data obtained here and especially the large value of 10 Dq (2 eV) determined in section 4.1 confirms the presence of a strong crystal field in the octahedral sites of the α-$ZnAl_2S_4$ host lattice occupied by Cr^{3+} impurities.

The dependence of the extrinsic PL intensity on excitation light intensity was determined at 298 K and 528 K in the hopes of observing the presence of stimulated emission. At both temperatures the behavior of the total extrinsic emission changed at a critical excitation intensity I_c of 2 MW/m^2. At a temperature of 298 K the rate of increase of the total emission abruptly augmented at I_c due to the appearance of emission from the $^4T_{2g}$ state and the Cr^{4+} centers. On the other hand at 528 K the total near IR emission was saturated past I_c indicating all the radiative levels of the Cr^{3+} centers were filled and that there was an increase of non-radiative transitions. Next, time-resolved measurements supplied the time decay of the luminescence between 2 K and 530 K. A four-level model for the radiative processes was proposed from which an equation was obtained and fitted to the time decay dependence on temperature. The fit produced the lifetimes of the radiative states and their energy differences. The time decay dependence on excitation intensity was also investigated at room temperature. For low excitation intensities the time decay was constant but it started decreasing rapidly above I_c.

The observed change of behavior in the extrinsic PL at I_c was an indication for the onset of stimulated emission. This was verified by optical gain measurements. The emission attributed to a Cr^{4+} center showed population inversion up to at least 378 K around 850 nm. Gain from the Cr^{3+} center was observed at room temperature with a

value of 8 cm^{-1} and showed a maximum value of 25 cm^{-1} at 730 nm at 198 K. The population inversion from the chromium impurities was suggested to take place via the $^4T_{2g} \rightarrow {}^4A_{2g}$ transition according to the four-level model described in section 2.5. The gain values observed in $ZnAl_2S_4$:Cr are small compared to certain semiconductors like CdS, with gain values of the order of 1200 cm^{-1} [28], but they are also 1 to 2 orders of magnitude larger than the gain values observed in ruby (0.3 cm^{-1} [29]) and $CdIn_2S_4$ (2.2 cm^{-1} [26]).

These results are promising for achieving laser action at room temperature and above. However further investigation of the inversion of population attributed to the Cr^{4+} centers at high temperatures would be interesting. The energy states of Cr^{4+} ions also need to be determined by measurements further into the near IR. Subsequent experiments could also be done on some new $ZnAl_2S_4$:Cr crystals with different chromium impurity concentrations to find the optimum concentration for a larger emission. Hopefully some larger crystals could make more precise measurements of optical gain possible.

REFERENCES

1. Kulikova, O.V., Kulyuk, L.L., Moldovyan, N.A., Popov, S.M., Remengo, D.S., Siminel, A.V., Proc. 8th Int. Conf. Ternary and Multinary Compounds, Kishinev, September 1990 (Moldavian Acad. Sci., 1991) p. 353
2. Kai, T., Kaifuku, M., Aksenov, I., Sato, K., Jpn. J. Appl. Phys. Vol. **34**, 3073 (1995).
3. Kulikova, O.V., Moldovyan, N.A., Popov, S.M., Radautsan, S.I., Siminel, A.V., Jpn.J.Appl.Phys., **32**, Suppl. 32-3, 586 (1993).
4. Duarte, F.J., Tunable Lasers Handbook, Academic Press, San Diego, 1995
   Berthold, H.J., Köhler, K., Z.anorg. allg. Chem., **475**, 45 (1981).
5. Kittel, Charles, Introduction to Solid State Physics, John Wiley & Sons, Inc., New York, 1996.
6. Beauvais, J., Fortin, E., Kulyuk, L , Tezlevan, V., Solid State Commun., **79**, 435 (1991).
7. Kulikova, O.V., Kulyuk, L.L., Popov, S.M., Tezlevan, V.E. and Fortin, E., Jpn.J.Appl.Phys., **32**, Suppl. 32-3, 484 (1993).
8. Berthold, H.J. and Kohler, K., Anorg. Z., Chem., **475**, 45 (1981)
9. Hahn, H. and Klingeler, W., Z, Anorg. Allg. Chem., **263**, 177 (1950)
10. Sugano, S., Tanabe, Y. and Kamimura, H., Multiples of Transition Metal Ions in Crystals. Academic Press, New York, 1970
11. Schläfer, Hans L. and Gliemann, Güner, Basic Principles of Ligand Field Theory, Wiley-Interscience, London (1969).
12 Figgis, B.N., Introduction to Ligand Fields, Robert E. Krieger Publishing Company, Malabar, Florida (1986).
13. Rasheed, F., O'Donnell, K.P., Henderson, B. and Hollis, D.B., J. Phys.: Condens. Matter, **3** 1915-1930 (1991)
14. Rebane K.K., Impurity Spectra of Solids, Plenum Press, New York and London (1970).
15. Boulon, G., Pedrini, C., Guidoni, M., Pannel, Ch., J. de Physique **26**, 266 (1975).

16. Zhang, Z.Y., Grattan, K.T.V., Palmer, A.W., J. Appl. Phys. **73**, 3493 (1993).

17. Zhang, Z.Y., Grattan, K.T.V., Palmer, A.W., Phys. Rev., **b48**, 7772 (1993).

18. Shaklee, K.L., Nahory, R.E. and Leheny, R.F., J. Lumin., 7, 284 (1973).

19. Kulikova, O.V., Kulyuk, L.L., Popov, S.M., Radautsan, S.I. and Tazlavan, V.E., Institute of Applied Physics, Academy of Sciences of Moldova.

20. G. and A.M. Lamarche, University of Ottawa, Canada.

21. Pedrotti, F.L. and Pedrotti, L.S., Introduction to Optics, Prentice-Hall, Englewoods Cliffs, 1987

22. Ueno, M., J.Phys.Soc.Jpn., **46**, 1877 (1979).

23. Graber, N., Orfino, F. and Schwerdtfeger, C.F., Solid State Commun., **36**, 407 (1980).

24. Jia, W., Liu, H., Jaffe, S. and Yen, W.M., Physical Review B, **43**, 7 (1991).

25. Pollock, C.R., Barber, D.B., Mass, J.L. and Markgraf, S., IEEE J. selected topics in Quantum Elec., Vol. 1, No. 1, April 1995.

26. Beauvais, J. and Fortin, E., J. Appl. Phys., **62** (4), August 1987.

27. Anedda, A., Fortin, E., J. Phys. Chem. Solids, Vol. **40**, 653 (1979).

28. Cingolani, A., Ferrara, M. and Lugrara, M., Optics communications, Vol. 34, 1 (1980).

29. Beauvais, J., Masters thesis, University of Ottawa, 1987.

IMAGE EVALUATION
TEST TARGET (QA-3)

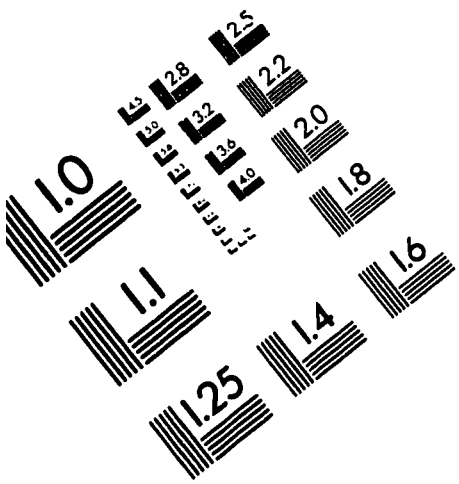

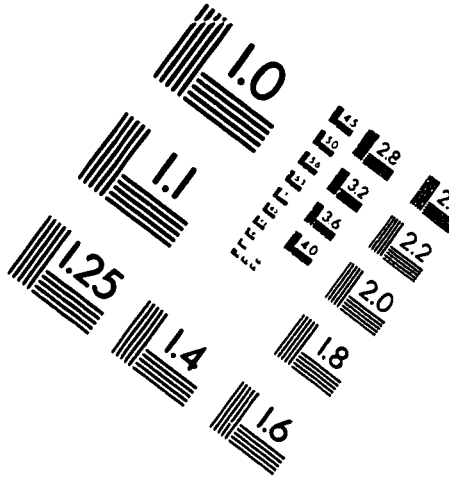

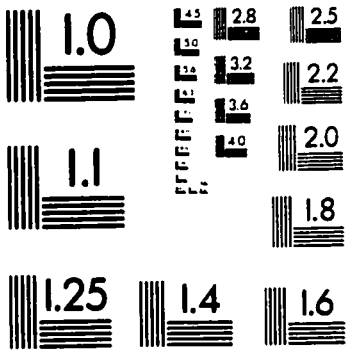

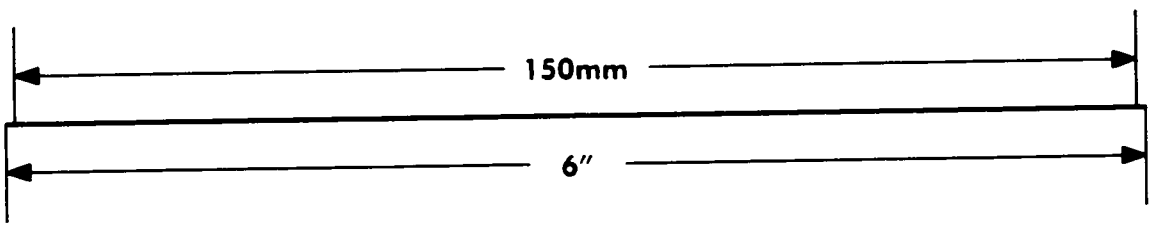

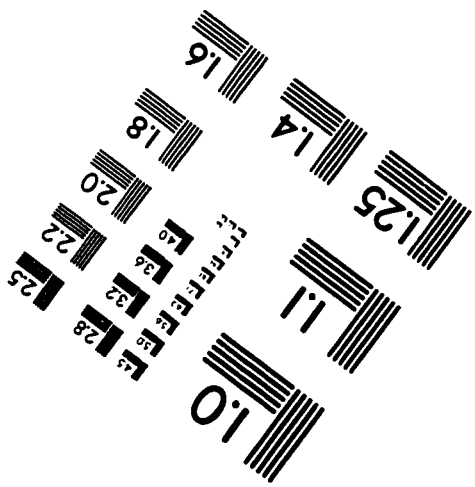

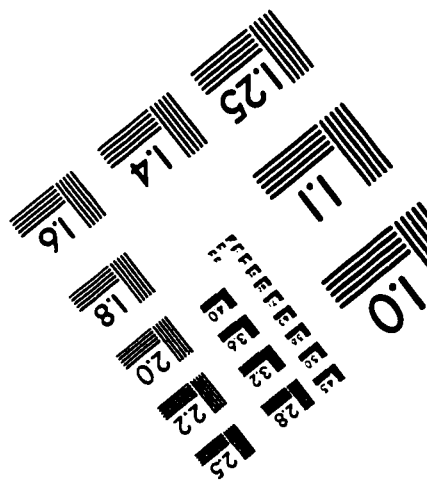

APPLIED IMAGE, Inc
1653 East Main Street
Rochester, NY 14609 USA
Phone: 716/482-0300
Fax: 716/288-5989